Simulations of Inositol Phosphate Metabolism and Its Interaction with $InsP_3$-Mediated Calcium Release

Jyoti Mishra and Upinder S. Bhalla
National Centre for Biological Sciences, GKVK Campus, Bangalore 560065, India

ABSTRACT Inositol phosphates function as second messengers for a variety of extracellular signals. Ins(1,4,5)P_3 generated by phospholipase C-mediated hydrolysis of phosphatidylinositol bisphosphate, triggers numerous cellular processes by regulating calcium release from internal stores. The Ins(1,4,5)P_3 signal is coupled to a complex metabolic cascade involving a series of phosphatases and kinases. These enzymes generate a range of inositol phosphate derivatives, many of which have signaling roles of their own. We have integrated published biochemical data to build a mass action model for $InsP_3$ metabolism. The model includes most inositol phosphates that are currently known to interact with each other. We have used this model to study the effects of a G-protein coupled receptor stimulus that activates phospholipase C on the inositol phosphates. We have also monitored how the metabolic cascade interacts with Ins(1,4,5)P_3-mediated calcium release. We find temporal dynamics of most inositol phosphates to be strongly influenced by the elaborate networking. We also show that Ins(1,3,4,5)P_4 plays a key role in $InsP_3$ dynamics and allows for paired pulse facilitation of calcium release. Calcium oscillations produce oscillatory responses in parts of the metabolic network and are in turn temporally modulated by the metabolism of $InsP_3$.

INTRODUCTION

Hormones, neurotransmitters, and growth factors that activate phospholipase C generate a bifurcating signal with Ins(1,4,5)P_3 at one arm and diacylglycerol (DAG) at the other (Rhee, 2001). Although DAG activates protein kinase C (Nishizuka, 1988), $InsP_3$ mobilizes calcium via the endoplasmic reticulum based $InsP_3$ receptor (Berridge, 1993). Intracellular levels of these secondary messengers depend on a balance between their rate of formation and rate of removal, which channels them back to lipid resynthesis. Ins(1,4,5)P_3 is metabolized in cells by an interplay of phosphatases and kinases (Shears, 1989) that result in production of inositol phosphates ranging from inositol monophosphates to inositol heptaphosphates and octaphosphates (Irvine and Schell, 2001). Understanding the kinetics of this complex metabolic network for $InsP_3$ is fundamental to deciphering its role in shaping intracellular calcium dynamics.

$InsP_3$ functions as an important secondary messenger (Berridge and Irvine, 1989; Streb et al., 1983) that binds to $InsP_3$ receptors embedded in the endoplasmic reticular membrane and mediates calcium release into the cytosol (Taylor and Richardson, 1991). This release can elevate calcium from 10 to 100 nM basal levels to several micromolar stimulated levels (Bootman and Berridge, 1995). Depending on the cell type, the calcium waveform can either exhibit a single peak or can oscillate with multiple spikes (Berridge and Irvine, 1989; Tsien and Tsien, 1990; Meyer and Stryer, 1991). Isolated calcium puffs generated locally in the cytosol can propagate throughout the cell as waves (Lechleiter et al., 1991; Parker and Yao, 1991) and activate various cell physiological processes (Berridge, 1993) including differentiation, proliferation, vesicle release, and sensory perception.

Like $InsP_3$, its metabolic products also play essential roles in cellular function, although they have not been as rigorously assessed as $InsP_3$. For instance, evidence has been accumulating for the role of Ins(1,3,4,5)P_4 in facilitating $InsP_3$-mediated Ca^{2+} release (Morris et al., 1987; Cullen et al., 1990; Smith et al., 2000). It was recently shown that calcium release activated calcium current (I_{CRAC}) (Hoth and Penner, 1992) is enhanced due to the inhibitory effect of Ins(1,3,4,5)P_4 on $InsP_3$ 5-phosphatase (Hermosura et al., 2000). The Ras signaling pathway is also affected by Ins(1,3,4,5)P_4 function. GTPase activating proteins, GAP1m and GAP1IP_4BP, gain activity by specifically binding $InsP_4$ (Cullen et al., 1995; Fukuda and Mikoshiba, 1996).

Ins(3,4,5,6)P_4 also functions as a secondary messenger that regulates calcium activated chloride efflux. It inhibits a plasma membrane chloride channel (Vajanaphanich et al., 1994; Shears, 1998) and is thus involved in osmoregulation. Further, its cellular levels are modulated by an $InsP_3$ isoform Ins(1,3,4)P_3, which is generated by the degradation of Ins(1,3,4,5)P_4 (Yang et al., 1999).

$InsP_5$ and $InsP_6$ (phytic acid) belonging to the inositol high polyphosphate series (IHPS), play essential regulatory roles in endocytosis and exocytosis. In vitro, they have been shown to interact in varying affinities with assembly proteins important in clathrin-mediated endocytosis and with synaptotagmin domains involved in synaptic vesicle trafficking (Fukuda and Mikoshiba, 1997). "High energy" pyrophosphates are equally important for intracellular trafficking. PP-$InsP_5$ is the most potent known inhibitor of AP-180-

Submitted January 16, 2002, and accepted for publication May 17, 2002.

Address reprint requests to Jyoti Mishra, National Centre for Biological Sciences, GKVK Campus, P.O. BOX 6501, Bangalore 560065, India. Tel.: 91-80-363-6420, ext. 3231; Fax: 91-80-363-6662; E-mail: jyoti@ncbs.res.in.

0006-3495/02/09/1298/19 $2.00

mediated clathrin cage assembly (Ye et al., 1995). There is also evidence that $InsP_5$ and $InsP_6$ may function as extracellular signals to regulate blood pressure and heart rate (Vallejo et al., 1987).

In addition to these specific signaling actions, inositol phosphates have also been shown to bind crucial cellular proteins like the cytoskeletal element vinculin, the signaling molecule Bruton's tyrosine kinase (Btk), and the cell adhesion molecule myelin proteolipid protein (Fukuda and Mikoshiba, 1997). Active research is being conducted to find the exact physiological significance of these varied binding properties of inositol phosphates.

In parallel with research on the functional relevance of inositol phosphates, several key enzymes in the metabolic cascade of $InsP_3$ have been identified (Majerus, 1992). These enzymes regulate the cellular concentrations of inositol phosphates under basal and stimulated conditions. They are all kinases and phosphatases that sequentially add or remove phosphate groups from the inositol ring, exhibiting high specificity for their substrates. They show extensive cross-talk among themselves and are subjected to regulation by inositol phosphates in the metabolic network that are not their immediate substrates and products. Some of these enzymes are also regulated by general signaling molecules such as calcium, protein kinase C (Sim et al., 1990), calmodulin (CaM), and calcium-calmodulin activated protein kinase type II (CaMKII) (Communi et al., 1997). Another dimension to interactions among inositol phosphate metabolism enzymes is their varied spatial distribution (Soriano et al., 1997). Most of them are present in the cytosol but some are attached to the plasma membrane whereas others such as multiple inositol polyphosphate phosphatase are compartmentalized in the ER (Chi et al., 2000; Nogimori et al., 1991). This distribution alters accessibility toward substrates and regulatory molecules. Further complexities arise because of the presence of multiple isoforms of the same enzymes, whose expression levels differ from one cell type to another. Although most of these kinases and phosphatases have strict substrate specificity, some also catalyze multisubstrate reactions.

We have constructed a biochemical model for the cellular metabolism of $Ins(1,4,5)P_3$. To generate the mass action model, we have made use of published biochemical data (see Supplementary Information) on enzyme purification and characterization, primarily from brain tissue studies. For understanding how metabolism modulates the levels of the various inositol phosphates under basal or stimulated conditions, the inositol phosphate network has been integrated with an existing model for $Ins(1,4,5)P_3$ generation via phospholipase Cβ activation (Bhalla and Iyengar, 1999). Stimulation is provided to the system as an external square pulse of glutamate transduced via the metabotropic glutamate receptor.

$InsP_3$ releases calcium from ER stores, and calcium can feed back onto both the production and degradation of $InsP_3$ (Harootunian et al., 1991; Communi et al., 1997). To account for this feedback, we incorporated a simplified model for the $InsP_3$ receptor and for calcium homeostasis. We found that the simple $InsP_3$ receptor model with a single $InsP_3$ binding step and no calcium feedback onto the receptor can only generate a nonoscillatory calcium response. Hence, to study interactions between $InsP_3$ metabolism and oscillatory calcium dynamics we adapted an existing model for detailed $InsP_3$ receptor kinetics developed by Othmer and Tang (Tang et al., 1996). The Othmer-Tang model incorporates both positive and negative Ca^{2+} feedback onto the $InsP_3$ receptor and produces periodic calcium spikes upon stimulation of $InsP_3$ levels.

Simulations of our $InsP_3$ metabolism model allow us to gauge how various inositol phosphates respond to a G-protein coupled receptor (GPCR) stimulus as a function of both concentration and time. We find that the response of $InsP_3$ is modified both by the presence of its metabolic cascade and by oscillations of calcium. $Ins(1,3,4,5)P_4$ emerges as a prominent regulatory molecule both for $InsP_3$ dynamics and calcium release.

MATERIALS AND METHODS

A block diagram representation of the $InsP_3$ metabolism model is presented in Fig. 1 *A*. Stimulus to the model was provided via glutamate (Glu) at the metabotropic glutamate receptor (mGluR). This lead to binding of GTP to the Gα subunit of G-protein. The activated G-protein then activated phospholipase C (PLC) β, which generated $InsP_3$ and DAG from phosphatidylinositol bisphosphate (PIP_2). Whereas DAG activated PKC, stimulated levels of $InsP_3$ acted on the ER $InsP_3$ receptor and released stored Ca^{2+}. Calcium, in turn, activated CaM, CaMKII, and PKC, which regulated $Ins(1,3,4,5)P_4$ formation among the higher phosphates. Ca^{2+} also activated PLC β by positive feedback and modulated enzymes within the lower inositol phosphate cascade. Termination of the GPCR signal was accelerated by the GTPase-activating protein (GAP) activity of PLC β.

Fig. 1 *B* illustrates details of inositol phosphate metabolism that were incorporated in our model. The metabolism of $Ins(1,4,5)P_3$ was modeled as a network of enzymes, including details of the regulation of these enzymes. As shown in Fig. 1 *B*, there were numerous instances of enzyme regulation by competitive inhibition from different inositol phosphates. Detailed regulation of $InsP_3$ 3-kinase via CaM binding and phosphorylation by PKC and CaMKII was also part of the model. Interactions among members of the network model were represented as chemical reactions that were either simple reactions characterized by a K_d (dissociation constant) or a K_{eq} (equilibrium constant) (Eq. 1) or were enzymatic reactions.

Simple reactions were of the form:

$$A + B \underset{k_b}{\overset{k_f}{\rightleftharpoons}} C \qquad K_d = k_b/k_f; \quad \tau \cong 1/(k_f + k_b) \quad (1)$$

In this formulation, interactions are completely specified by the initial concentrations of the reactants (A and B) and the product (C), by the rate constant for the forward reaction, k_f, and the rate constant for the back reaction, k_b. τ represented the time course of the simple reaction. Its exact value, which can be influenced by various factors in a reaction network, was initially approximated during model building and subsequently validated through simulations.

Eq. 1 can also be represented as a differential equation given by: $d[A]/dt = -k_f[A][B] + k_b[C]$ and similar equations for the other molecules that participate in the reaction.

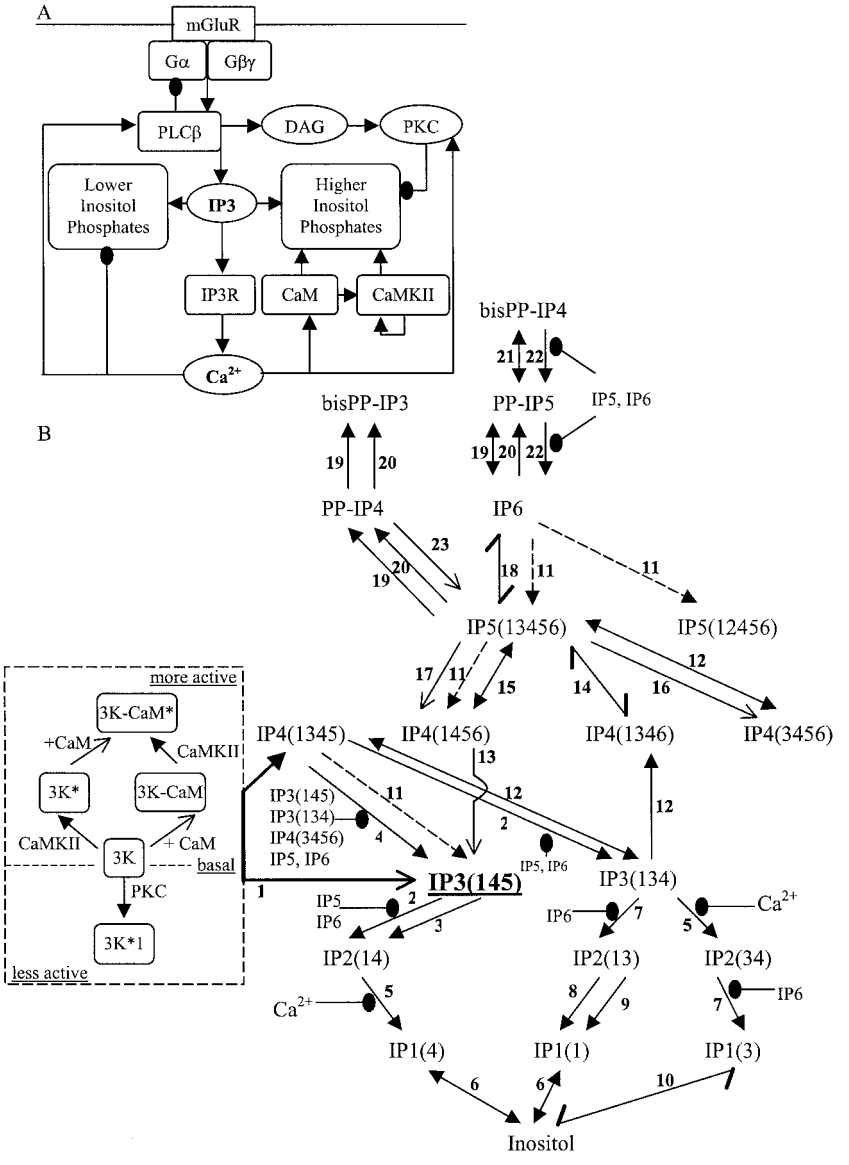

FIGURE 1 (*A*) Block diagram of complete model. The glutamate stimulus is provided at the metabotropic glutamate receptor (mGluR). G-protein activated PLC β generates $InsP_3$ and DAG from PIP_2. The GAP activity of PLC β accelerates termination of the G-protein signal. Whereas DAG activates PKC, $InsP_3$ acts on the ER $InsP_3$ receptor and releases Ca^{2+} from stores. Stimulated levels of cytosolic calcium activate Calmodulin, CaMKinase II, and PKC, which regulate Ins(1,3,4,5)P_4 formation among the higher phosphates. Ca^{2+} also has positive feedback onto PLC β and modulates enzymes within the lower phosphate cascade. →, Activation; —● inhibition. (*B*) Diagram representing modeled details of $InsP_3$ metabolism. Pointer symbols used are as follows: →, Michaelis-Menten enzymes; ◄►, reversible enzymes; ⇐►, enzymes that have Michaelis-Menten kinetics in the basal form but are reversible in the activated form; ⟹, simple reactions; ⇄, reversible simple reactions; —●, competitive enzyme inhibition; ⇢, a composite process where substrate is transported to ER, reaction is catalyzed by ER based enzyme, and product is transported back to the cytosol. Numbers next to symbols depict enzyme/reaction names. Identical numbering on different enzyme reactions indicates that the same enzyme catalyzes many unique reactions with distinct rates for each conversion. Multiple pointer symbols from one inositol phosphate to another represent the different ways in which the same interconversion is achieved. The box on the left depicts Ins(1,4,5)P_3 3-kinase and covalent modifications to it by PKC, CaM, and CaMKII, that modify enzyme activity as shown. 1, Ins(1,4,5)P_3 3-kinase; 2, InsP 5-phosphatase1; 3, Ins(1,4,5)P_3 5-phosphatase2; 4, Ins(1,3,4,5)P_4 3-phosphatase; 5, InsP 1-phosphatase; 6, $InsP_1$ phosphatase; 7, InsP 4-phosphatase; 8, Ins(1,3)P_2 3-phosphatase1; 9, Ins(1,3)P_2 3-phosphatase2; 10, Ins(3)P_1 phosphatase; 11, multiple inositol polyphosphate phosphatase; 12, Ins(1,3,4)P_3 5,6-kinase/Ins(3,4,5,6)P_4 1-kinase/$InsP_5$ 1-phosphatase; 13, Ins(1,4,5,6)P_4 6-phosphatase; 14, Ins(1,3,4,6)P_4 5-kinase, 15, Ins(1,4,5,6)P_4 3-kinase; 16, $InsP_5$ 1-phosphatase; 17, $InsP_5$ 3-phosphatase; 18, $InsP_5$ 2-kinase/$InsP_6$ 2-phosphatase; 19, $InsP_6$ kinase1; 20, $InsP_6$ kinase2; 21, PP-$InsP_5$ kinase; 22, Diphosphoinositol polyphosphate phosphohydrolase; 23, PP-$InsP_4$ phosphatase.

Enzyme reactions modeled in the network mostly followed Michaelis-Menten kinetics (Eq. 2), but some enzymes were modeled with reversible kinetics.

The Michaelis-Menten scheme for enzyme-catalyzed reactions was of the form:

$$E + S \underset{k_2}{\overset{k_1}{\rightleftharpoons}} ES \xrightarrow{k_3} E + P \qquad K_m = (k_2 + k_3)/k_1; \quad V_{max} = k_3 \tag{2}$$

This standard formulation for enzymes is a special case of two reactions in sequence with the assumption that the final step is irreversible. It is specified by three rate constants k_1, k_2, and k_3, and the initial concentrations of the enzyme *E*, substrate *S*, and product *P*. Unless actual rate constants were provided in literature, k_2 was taken as four times k_3. Most enzyme models are insensitive to the exact value of this ratio (Bhalla, 1998). We validated this in our model also by testing k_2:k_3 ratios ranging from 0.4 to 40 without significant variation in simulation results (data not shown).

Reversible enzyme reactions were of the form:

$$E + S \underset{k_2}{\overset{k_1}{\rightleftharpoons}} ES \underset{k_4}{\overset{k_3}{\rightleftharpoons}} E + P$$

$$K_m^s = (k_2 + k_3)/k_1; \quad K_m^p = (k_3 + k_2)/k_4; \quad V_{max}^s = k_3 - k_2; \quad V_{max}^p = k_2 - k_3 \tag{3}$$

Here K_m^s and K_m^p represent the distinct affinities of the enzyme for the substrate and product respectively, and V_{max}^s and V_{max}^p represent the maximal velocities of the forward and backward reactions. Enzymes were modeled as reversible reactions when the back flux from the reaction

TABLE 1 Parameter set used to model $InsP_3$ dephosphorylation by InsP 5-phosphatase1 and its inhibition by $InsP_5$

Molecule	Initial concentration (μM)	Buffering*	Notes
IP_5pase1	12.346	0	InsP 5-phosphatase1 enzyme pool: from Hansen et al., 1987.
IP5(13456)	53.999	0	Ins(13456)pentakisphosphate: concentration from Voglmaier et al., 1996.
IP5-5pase-cmplx	0	0	Product complex of the competitive enzyme inhibition reaction of IP5 with IP_5pase1.

Reaction	K_f	K_b	Notes
IP5-inhib-3pase	1	0.06	Reaction for competitive inhibition of IP_5pase1 by IP5: Ki from Hoer and Oberdisse, 1991.

Enzyme	Parent	K_m	V_{max}	Ratio†	Notes
ip3_5pase1	IP_5pase1	3	1.1	4	Ins(145)P3 5-phosphatase activity of InsP 5-phosphatase1: from Hansen et al., 1987.

*Buffering indicates whether a pool is held fixed at its initial concentration through simulation runs. For such pools buffering is 1.
†Value refers to ratio of k_2/k_3 for Michaelis-Menten enzymes (Eq. 2).

products to the substrates was over 5% of the forward flux. The value of the fourth rate constant k_4, unless available in literature, was derived by free energy calculations. For a reaction at equilibrium, the standard free energy change $\Delta G°$ (kJ/mol) is related to K_{eq} (equilibrium constant for the reaction) by:

$$\Delta G° = -RT \ln K_{eq}$$

$$R = 8.314 \text{ JK}^{-1} \text{ mol}^{-1}, \quad T = 310 \text{ K} \qquad (4)$$

Further K_{eq} is related to the rate constants of the reversible enzyme reaction by:

$$K_{eq} = (k_1 * k_3)/(k_2 * k_4) \qquad (5)$$

We extracted k_4 for each enzyme reaction for $\Delta G°$ values ranging from -10 kJ/mol to -25 kJ/mol. This $\Delta G°$ range was approximated from values for glucose phosphorylation (Jencks, 1976) as the $\Delta G°$ for phosphorylation of the inositol ring has not, to our knowledge, been reported in the literature. We chose a wide range of $\Delta G°$ values to span the likely range of k_4 rates. Glucose was chosen due to its structural similarity to inositol. This similarity is quite close, and in some cases glucose serves as a cellular precursor to inositol phosphates (Irvine and Schell, 2001).

In this way all enzyme reactions depicted in Fig. 1 *B* by ↔ symbols were modified from the Michaelis-Menten scheme to the reversible kinetics scheme. In general the reversibility of reactions did not introduce large changes in the model kinetics, but there are some interesting exceptions that are discussed in the Results section.

Parameters for all enzymes modeled were derived from published biochemical experiments that involve protein purification and characterization of enzyme kinetics. Michaelis-Menten enzymes were characterized by their K_m and V_{max}, and their initial concentrations were obtained from biochemical purification series and quantitative immunoprecipitation. In most cases, measurements across different published reports in literature allowed us to cross check the values of the constants we used. For simple reactions, k_f and k_b were constrained by time courses and dose response curves. Certain reactions within the inositol phosphate metabolic network that have been described in literature as enzymatic reactions but for which enzyme kinetics have not been characterized in mammalian systems had to be modeled as simple reactions. Rates for such reactions were constrained by equilibrium concentrations of their reactants and products. The incorporation of these simple reactions into the model introduces parameters that have not been tested experimentally. Nevertheless, the equilibria for these reactions are tightly constrained by the known steady-state levels of reactants in the $InsP_3$ metabolism cascade. Without these reactions, depicted in Fig. 1 *B* by numbers 10, 13, 14, 16, 17, 18, and 23, components of the metabolic network do not equilibrate in simulation runs due to unbalanced source-sink relationships among them. We acknowledge that precise kinetics of these reactions require validation through experiments.

Detailed parameters for all modeled reactions are presented in the Supplementary Information and on the DOQCS website (http://doqcs.ncbs.res.in, accession 31-32). A sample parameter set that describes enzyme 2 and its inhibition by $InsP_5$ in Fig. 1 *B* is shown in Table 1. Table 2 enumerates the total number of molecules, reactions, Michaelis-Menten enzyme activities, and channels present in our model. The non-Osc-model in Table 2 refers to a version of the network model wherein details of $InsP_3$ receptor kinetics were not incorporated and which showed nonoscillatory dynamics for $InsP_3$-mediated Ca^{2+} release. The Osc-model refers to the network model that included detailed $InsP_3$ receptor kinetics. In this model, kinetic parameters for the $InsP_3$ receptor were closely based on the Othmer-Tang calcium dynamics model (Tang et al., 1996). The Osc-model also differed from the non-Osc-model in basal Ca^{2+} levels and interactions between the ER sequestered and extracellular calcium pools. These parameter modifications were made with the sole objective to generate cytosolic Ca^{2+} oscillations and have been enumerated in the Supplementary Information.

Input to the signaling network was delivered as square pulses of glutamate at the mGluR. The model used for representing mGluR does not include receptor inactivation, desensitization, or receptor recycling details. It is an approximation of actual receptor kinetics intended to serve as a stimulus generator for the main focus of our model, $InsP_3$ metabolism. In our model, stimuli of amplitude ≥ 0.5 μM glutamate produced saturating responses. The system was allowed to settle to a steady state before being stimulated, and input delivery was followed by a poststimulatory run that ensured restoration of steady state.

TABLE 2 Total number of molecules, reactions, Michaelis-Menten enzyme activities, and channels present in the $InsP_3$ metabolism network models

Network	Molecules	Reactions	Enzyme activities	Channels
Non-Osc-model	135	90	42	4
Osc-model	138	91	43	4

A sensitivity analysis was performed to investigate how sensitive the model was to the numerous parameters used to build it. For this analysis, parameters were classified in five categories of initial concentration, reaction dissociation constant (K_d), reaction time course (τ), enzyme Michaelis constant (K_m), and enzyme maximal velocity (V_{max}). Values of all parameters in each category were systematically scaled 0.1, 0.2, 0.5, 0.667, 0.833, 1.2, 1.5, 2, 5, and 10 times their original value and the model subjected to simulation runs. Variability in results for this 100-fold range (0.1–10) of all parameter values were analyzed by generating scatter plots for logarithmic fold changes in outputs for calcium, $Ins(1,4,5)P_3$, $Ins(1,3,4,5)P_4$, and $Ins(1,3,4)P_3$. For the model that included detailed $InsP_3$ receptor kinetics, the scatter plot readout was the frequency of calcium spikes generated within stimulus time. For ease of analysis, all scatter plots were normalized with respect to the control output. The control refers to the basic scheme of the model with the original parameter values.

Two global sensitivity analyses were also performed to investigate the effects of alterations in a combination of parameters on the model behavior. The first global analysis focused on effects of temperature alteration on the system. This was based on the premise that an ~10°C rise in temperature accelerated reaction rates by twofold. Simulations were performed to assess the effects of 10°C rise and 10°C fall in temperature on all reaction rates. The second global sensitivity analysis targeted all energy consuming reactions, i.e., kinases and ATPases, which would be affected by ATP depletion in the system. Because for most reactions ATP was not explicitly included as a reactant species, a change in ATP concentration to x times its original value was approximated by scaling enzyme K_m by a factor of $1/x$, and by changing the k_f and k_b of ATP dependent reactions by a factor of x and $1/x$, respectively. Simulation runs were performed for ATP depletion to 0.5 and 0.15 times its original concentration, which represent physiological drops in cellular ATP levels (Kahlert and Reiser, 2000). Sensitivity analysis outputs were monitored for Ca^{2+}, $Ins(1,4,5)P_3$, $Ins(1,3,4,5)P_4$, and $Ins(1,3,4)P_3$ and are discussed at the end of the Results section.

All numerical computations were performed using a graphical interface–Kinetikit (version 7) on the General Neural Simulation System–GENESIS (Bhalla, 1998). Computations were carried out on PCs running Linux. The exponential Euler formulation was used for integration (MacGregor, 1987). Numerical accuracy of the computations was verified by comparing the results for simulations that had been run at different time steps. The model provided convergent solutions for the range of time steps used in the study. For analysis of the model output, a time step of 0.2 ms was used. At initiation of the simulation run and at all transient points wherein steady state of the model was perturbed by a stimulus input, a fine time step of 10 μs for 10 s was used. The temporal characteristics of some of the output curves are described in terms of rise time of the response to stimulus, response latency, and response width. We define rise time of a response to stimulus as the time taken to progress from 20% to 80% of the maximal response height. Response latency is defined by the time taken to achieve 20% of maximal response height from stimulus onset, and response width represents the full width of the response at half maximal response height.

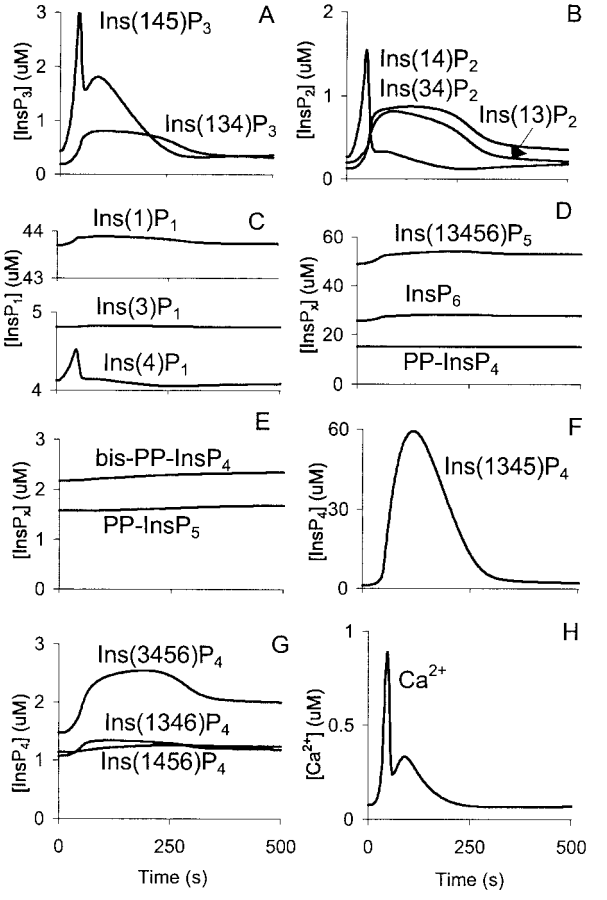

FIGURE 2 Responses of the various inositol phosphates in the non-Osc-model to a 30-s pulse of 0.5 μM glutamate. The concentration axis is scaled differently in each panel. Response latency (RL) and response width (RW) are calculated as described in the methods and reported for selected traces. (*A*) Responses of the two $InsP_3$ isoforms are markedly different. $Ins(1,4,5)P_3$ shows a fast transient response (RL, 22 s; RW, 20 s). $Ins(1,3,4)P_3$ has a slow prolonged rectangular response (RL, 32 s; RW, 246 s). (*B*) Responses of $InsP_2$s mimic responses of $InsP_3$s from which they are derived. (*C*) Responses of $InsP_1$s whose high basal levels are maintained by back flux from inositol. (*D* and *E*) Inositol high polyphosphates: $Ins(1,3,4,5,6)P_5$, $InsP_6$ and PP-$InsP_4$, and inositol pyrophosphates: PP-$InsP_5$ and bis-PP-$InsP_4$ show negligible stimulus responses. (*F*) $Ins(1,3,4,5)P_4$ shows the largest (60-fold) response to stimulus (RL, 52 s; RW, 139 s). (*G*) Responses of $InsP_4$s: $Ins(1,3,4,6)P_4$, $Ins(1,4,5,6)P_4$, and $Ins(3,4,5,6)P_4$, of which the $Ins(3,4,5,6)P_4$ response is physiologically important for chloride channel regulation. (*H*) Biphasic Ca^{2+} response to the $Ins(1,4,5)P_3$ generating stimulus.

RESULTS

Responses of components of the $Ins(1,4,5)P_3$ metabolic pathway

We first characterized the effects of a PLC β-activating stimulus on the components of the $Ins(1,4,5)P_3$ metabolism model. For this purpose, the non-Osc-model was initially allowed to achieve steady state by running the model without stimulation for a period of 1000 s. Stimulus was then provided as a square pulse of 0.5 μM glutamate for 30 s. Poststimulation model responses were simulated for 1000 s.

Components of the $InsP_3$ metabolic pathway showed varied responses to stimuli with respect to both amplitude and time of response. These are depicted in Fig. 2.

Responses of $Ins(1,4,5)P_3$ and its lower phosphates

$Ins(1,4,5)P_3$ responded to stimulus with a sevenfold concentration change. The half-life of $InsP_3$ has been estimated at 9 ± 2 s in N1E-115 neuroblastoma cells both by biochemical methods and by calcium imaging studies (Wang et

al., 1995). Our simulations generate a similar half-life value of 10 s for $InsP_3$. The simulated response width of $InsP_3$ was 20 s. The direct degradation product of $InsP_3$, $Ins(1,4)P_2$ showed a similar response width and a similar concentration change of approximately sixfold. The peak responses of these two inositol phosphates were sharp and transient and inactivated more rapidly than responses of other inositol phosphates. We found the kinetics of PLC β to be primarily responsible for the rapid peak transients of $InsP_3$ and its lower phosphates. The GTPase-activating protein activity of PLC β (Berstein et al., 1992) has been incorporated in our model. Thus, activated PLC β hastens inactivation of its stimulatory G-protein above its basal inactivation rate and in turn rapidly restores itself to its low V_{max} basal form. If this negative feedback GAP activity of PLC β is excluded from our model, the transient nature of $InsP_3$ and $Ins(1,4)P_2$ responses is lost (not shown).

Further, the $InsP_3$ response was observed to be biphasic with the rapid peak phase followed by a slow plateau-like phase at less than 50% the peak height. The second phase of the response was due to significant reverse flux in the phosphorylation reaction catalyzed by activated $InsP_3$ 3-kinase. This phase corresponds to the rapid increase in $Ins(1,3,4,5)P_4$ levels upon stimulation and is not seen if CaM- and CaMKII-activated $InsP_3$ 3-kinase is modeled as an irreversible Michaelis-Menten enzyme. The biphasic $InsP_3$ response directly correlates to a biphasic response for $InsP_3$ receptor released Ca^{2+} (see Fig. 2 *H*), which is observed under physiological conditions (Lambert and Nahorski, 1990). Characteristics of the Ca^{2+} response to stimulus are described in the following sections.

Responses of Ins(1,3,4)P_3 and its lower phosphates

$Ins(1,3,4)P_3$ responded to the 30-s 0.5 μM glutamate pulse with an approximately fourfold concentration change. Its dephosphorylation products, $Ins(1,3)P_2$ and $Ins(3,4)P_2$, showed similar responses with sixfold and fourfold changes in concentration, respectively. As seen in Fig. 2 *B*, the major route for $Ins(1,3,4)P_3$ metabolism was via Inositol phosphate 1-phosphatase, such that basal or stimulated levels of $Ins(3,4)P_2$ were always greater than levels of $Ins(1,3)P_2$. This metabolic predominance of $Ins(3,4)P_2$ has been reported experimentally (Bansal et al., 1987). Another characteristic of the $Ins(1,3,4)P_3$ response that tallies with experiments was its response latency (time taken to achieve 20% of maximal response height from stimulus onset). Our simulations generated a latency of ~30 s for $Ins(1,3,4)P_3$, which is 10 s longer than that for $Ins(1,4,5)P_3$. A comparable delay in $Ins(1,3,4)P_3$ build-up has been shown by Hughes and Drummond (1987) and Jackson et al. (1987). Their experiments suggest that this delay reflects the time taken for the receptor signal to progress from $Ins(1,4,5)P_3$ to $Ins(1,3,4,5)P_4$ and then to $Ins(1,3,4)P_3$ by the successive action of $InsP_3$ 3-kinase and InsP 5-phosphatase1. $InsP_3$ 3-kinase is a relatively fast enzyme but InsP 5-phosphatase1 activity for its $InsP_4$ substrate is slow and further inhibited by physiological levels of $InsP_5$ and $InsP_6$.

$Ins(1,3,4)P_3$ and its metabolites showed a prolonged rectangular concentration response over time, in contrast to the sharp transient responses of $Ins(1,4,5)P_3$. For $Ins(1,3,4)P_3$, this slow response had a width of ~250 s. Its peak concentration was maintained as a near plateau for 55% of this time. We observed that the time spent near peak directly overlapped with the response width of $Ins(1,3,4,5)P_4$. Fig. 2 *F* shows that upon stimulation, $Ins(1,3,4,5)P_4$ undergoes a 60-fold change in levels, which is the largest change seen for any inositol phosphate in the network. Such high $Ins(1,3,4,5)P_4$ levels serve as a nonlimiting substrate pool for generation of $Ins(1,3,4)P_3$ and its dephosphorylated products. Input to $Ins(1,3,4)P_3$ was both via dephosphorylation of $InsP_4$ by InsP 5-phosphatase1 and by the flux reversal in the phosphorylation reaction catalyzed by $InsP_3$ 5,6-kinase (Ho et al., 2002). Under the influence of saturating concentrations of $Ins(1,3,4,5)P_4$, enzymes downstream of it functioned at their respective V_{max}. This was seen not only at the primary level, i.e., conversion to $Ins(1,3,4)P_3$, but also at the secondary level, i.e., conversion of $Ins(1,3,4)P_3$ to $Ins(1,3)P_2$ and $Ins(3,4)P_2$. Thus, for ~140 s for which $InsP_4$ levels were elevated beyond 50% of its peak levels, $Ins(1,3,4)P_3$ and its metabolites maintained an elevated plateau phase. During this time we also observed a dip below basal levels for $Ins(1,4)P_2$. This was caused by high $Ins(1,3,4,5)P_4$ levels acting as potent substrate competitor for the enzyme InsP 5-phosphatase1, which catalyzes $Ins(1,4)P_2$ synthesis from $Ins(1,4,5)P_3$. Further consequences of this particular enzyme substrate competition on $Ins(1,4,5)P_3$ are elaborated in later sections of the paper.

Thus, we see that due to the networking within the inositol phosphate cascade, large scale changes in one component of the system, such as $Ins(1,3,4,5)P_4$, can have diverse effects on various other molecules. We predict $Ins(1,3,4,5)P_4$ to be a prominent modulator of the temporal characteristics of other inositol phosphates. The consequent prolonged elevation of $Ins(1,3,4)P_3$ and its derivatives can provide these molecules with a relatively long-term capacity for cellular function.

Responses of Ins(1,3,4,5,6)P_5 and other inositol high polyphosphates

The IHPs include $Ins(1,3,4,5,6)P_5$, $InsP_6$, PP-$InsP_4$, PP-$InsP_5$, and bis-PP-$InsP_4$. As seen in Fig. 2, *D* and *E*, their responses are negligible compared with those of the lower inositol phosphates. They seem to form a separate biochemical pool that is unaffected by the $Ins(1,4,5)P_3$ generating stimulus. This is probably because $InsP_5$ and $InsP_6$ have very large basal pools (30–60 μM) that may require strong direct stimulation for any appreciable changes to occur. Safrany and Shears (1998) have shown that a cAMP-mediated mechanism regulates the turnover of bis-PP-$InsP_4$,

which further suggests that the IHPs are regulated by other pathways than a PLC β signal. In an Ins(1,4,5)P_3 3-kinase overexpression study conducted in fibroblast cells (Balla et al., 1994), negligible increases in InsP_5 and InsP_6 concentrations had been reported. However, Balla et al. (1994) showed cell cycle dependent changes in the levels of these inositol phosphates. InsP_5 and InsP_6 increased markedly during the S-phase of the cell cycle. This further corroborates the role of regulators extrinsic to Ins(1,4,5)P_3 generation in influencing the IHPs. Because the exact molecular mediators that control levels of these inositol phosphates are not known, we do not include them in our model.

We have shown that the behavior of the IHPs in our model is concordant with experiments that analyze effects of GPCR stimuli on inositol phosphates. We further investigate what happens upon direct stimulation of IHPs in later sections of this paper.

Responses of inositol tetrakisphosphates

Within the whole InsP_3 metabolic cascade, the most prominent response was that of Ins(1,3,4,5)P_4. Stimulation produced a 60-fold change in Ins(1,3,4,5)P_4 concentration, which developed with a rise time of ~30 s. This large change was primarily because of the extensive positive regulation of the InsP_4 synthesizing enzyme, InsP_3 3-kinase, by calmodulin and CaMKII (Communi et al., 1997), which themselves undergo activation by Ca^{2+} under stimulated conditions. Compared with the approximately sixfold activation of Ins(1,4,5)P_3's dephosphorylation product Ins(1,4)P_2, stimulation of Ins(1,3,4,5)P_4, InsP_3's phosphorylation output was much greater. Thus, we conclude that phosphorylation was the predominant means of Ins(1,4,5)P_3 metabolism in our system.

The complete Ins(1,3,4,5)P_4 response was bell shaped with a response width of ~140 s. As mentioned earlier, the InsP_4 response heavily influenced the responses of other inositol phosphates, especially Ins(1,3,4)P_3 and its dephosphorylated products. The large build-up of InsP_4 levels in the metabolic pipeline affected enzymes downstream of it such that they function near their respective V_{max}. Thus, stimulus responses for Ins(1,3,4)P_3 and others were rectangular rather than expected bell shapes. We further verified that Ins(1,3,4,5)P_4 was responsible for this phenomenon. For this, we incorporated a new kinetic pool in our model that served as a drainage sink for InsP_4 outside of the inositol phosphate network. This pool did not allow InsP_4 levels to exceed fivefold above basal, upon stimulation. Simulations of this model showed that in presence of the external InsP_4 sink, responses of Ins(1,3,4)P_3 and its derivatives were like the sharp transient responses of Ins(1,4,5)P_3 (not shown). Further, the difference in response latencies of the Ins(1,3,4)P_3 and Ins(1,4,5)P_3 responses was also lost. Thus, in tissues such as the brain where Ins(1,4,5)P_3 3-kinase levels are high and large amounts of Ins(1,3,4,5)P_4 are generated, InsP_4 may function as an important temporal regulator for the other inositol phosphates.

Ins(3,4,5,6)P_4 displayed a ~2-fold response to stimulus. This InsP_4 is synthesized from InsP_5 by a reversible kinase/phosphatase, which also phosphorylates Ins(1,3,4)P_3 (Yang and Shears, 2000; Ho et al., 2002). However, experimentally reported basal and stimulated levels of Ins(3,4,5,6)P_4 could not be generated by this enzyme in our model system. For this purpose, a separate InsP_5 1-phosphatase reaction was incorporated into the network. The temporal response of this InsP_4 followed that of InsP_5 and was rectangular in shape. InsP_5 receives input from the lower inositol phosphate Ins(1,3,4)P_3 via phosphorylation of Ins(1,3,4,6)P_4. It was interesting to note that the rectangular shape of the temporal response of Ins(1,3,4)P_3 could be faithfully transmitted to Ins(3,4,5,6)P_4, which is at a tertiary interaction level in the network (see Fig. 1 *B*). Further, the width of the Ins(3,4,5,6)P_4 response was ~410 s. Such long-term elevation in Ins(3,4,5,6)P_4 levels has been reported experimentally (Pittet et al., 1989) and is important for its cellular function as an inhibitor of Ca^{2+} activated chloride efflux (Vajanaphanich et al., 1994).

Ins(1,3,4,6)P_4 showed a negligible response to stimulus, which is concordant with the measure of its stimulated levels in cerebral-cortex slices (Batty et al., 1989). Similarly response of Ins(1,4,5,6)P_4 was also negligible. This was because its only input was from the negligibly stimulated InsP_5 pool, but unlike its counterpart Ins(3,4,5,6)P_4 that receives similar input, this pool rapidly drained out into the lower inositol phosphates by the InsP_4 6-phosphatase reaction.

Calcium response in the model and incorporation of oscillations

The primary function of Ins(1,4,5)P_3 as a secondary messenger is to release calcium from intracellular stores in response to external stimuli. We used a 0.5-μM glutamate stimulus lasting 30 s to monitor the calcium output. As seen in Fig. 2, the biphasic InsP_3 response to stimulus in the non-Osc-model resulted in biphasic calcium release. Such a response with an early peak phase followed by a lower plateau-like phase has been reported for calcium under physiological conditions (Lambert and Nahorski, 1990). Peak stimulated levels of Ca^{2+} reached ~0.9 μM and were ~12-fold above basal.

Various mechanisms have been hypothesized for the periodic oscillations of cytosolic calcium seen in different cell types (Berridge, 1990). Positive feedback of calcium onto PLC β that generates InsP_3 underlies the calcium oscillation mechanism shown in certain experiments (Harootunian et al., 1991) and models (Meyer and Stryer, 1988). Although our non-Osc-model incorporated such feedback, it failed to display Ca^{2+} oscillations. This probably resulted from different parameter representations across models and cell types. Hence, to study interactions between molecules in the inositol phosphate metabolic cascade and oscillatory calcium dynamics, we appended

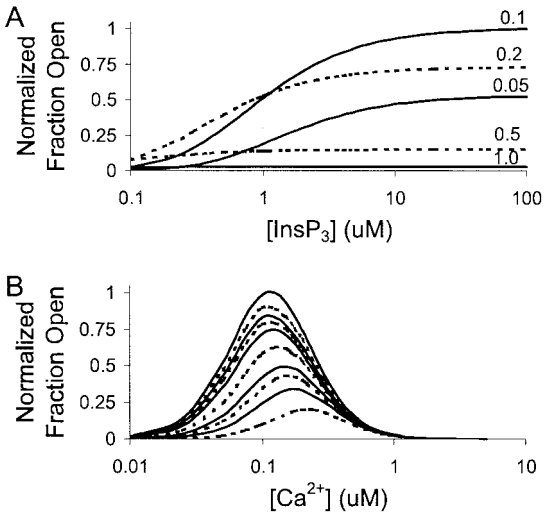

FIGURE 3 Responses of the $InsP_3$ receptor (kinetics adapted from the Othmer-Tang model) as a function of (*A*) $InsP_3$ concentration and (*B*) Ca^{2+} concentration. Ca^{2+} levels in μM used in *A* to generate the $InsP_3$ function curves are shown on the graph. $InsP_3$ levels used in *B* to generate the Ca^{2+} function curves (from the lowermost curve upward) are: 0.25, 0.5, 0.75, 1.0, 2.0, 5.0, 10, 20, 50, and 100 μM, as alternating dashed and solid lines, respectively. Concentration (μM) values represented on the *x* axis are on a logarithmic scale. Values on the *y* axis represent the steady-state concentration of active $InsP_3$ channels normalized against the maximal concentration of active channels obtained with 0.1 μM Ca^{2+} in *A* and 100 μM $InsP_3$ in *B*. The maximal percentage of channels open in *A* and *B* are 8% and 9.5%, respectively.

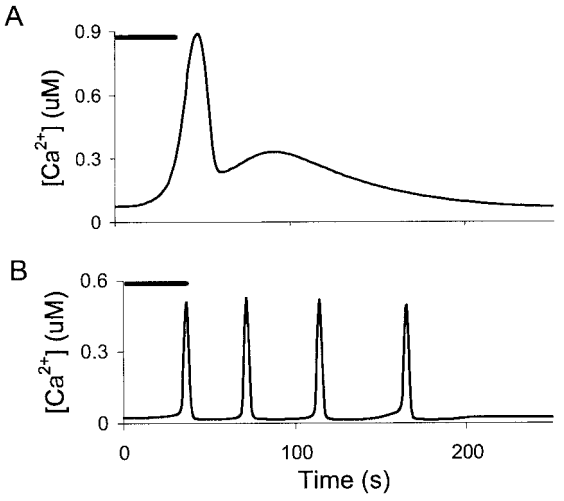

FIGURE 4 Comparison of Ca^{2+} responses generated in the (*A*) non-Osc-model and (*B*) Osc-model to a 30-s 0.5 μM glutamate stimulus (*solid bar*).

the Othmer-Tang calcium oscillation model (Tang et al., 1996) to our $InsP_3$ metabolism model. As mentioned previously in the Materials and Methods section, we refer to the resultant composite model as the Osc-model. The Othmer-Tang model is characterized by both a positive and a negative feedback from calcium onto its store release channel, the $InsP_3$ receptor. The channel in its conducting state has both calcium and $InsP_3$ bound. This mobilizes calcium from the ER to the cytosol. An excess calcium accumulation in the cytosol results in more calcium being bound to the receptor. This leads to channel inactivation.

The $InsP_3$ receptor response to increasing $InsP_3$ and calcium concentrations, in the nanomolar to micromolar range, was plotted as the normalized fraction of channels open versus the log of concentration (Fig. 3). The plots show a bell-shaped curve for $InsP_3$ receptor response to calcium, and a saturating curve reflects dependence of response on $InsP_3$ input. These are similar to the plots generated by Tang et al. (1996).

In our Osc-model basal calcium levels are ~20 nM, which is below the physiological range. Low basal calcium levels close to 0 nM are also used by Othmer and Tang for their model and are necessary for sustaining the oscillatory response. For maintaining calcium at such low levels we had to modify parameters for interactions between cytosolic and extracellular calcium, such as the store-operated calcium entry and the plasma membrane calcium pump (see Supplementary Information). These parameters may not be an accurate representation of experimental observations.

A comparison of the calcium responses within the non-Osc-model and the Osc-model to the 30-s stimulus pulse of 0.5 μM glutamate is provided in Fig. 4. The single calcium transient in the non-Osc-model is replaced by four calcium spikes in the Osc-model. These two models are used separately to study interactions between calcium and $InsP_3$ metabolism in further sections of this paper. Below we shall also analyze the differences that arise in these interactions due to the oscillatory nature of calcium.

Effects of glutamate stimulus intensity on $InsP_3$ buildup and calcium release

Cellular systems respond differently to different intensities of stimuli. The input parameters can modulate the output in terms of amplitude, time, and frequency of response. Here we analyze effects of different intensities of the glutamate stimulus on $InsP_3$-mediated calcium release. Fig. 5 *A* shows the calcium response within the non-Osc-model to 30-s pulses of glutamate stimuli of magnitude: 5 nM, 10 nM, 50 nM, 0.1 μM, and 0.5 μM. The time curves show that increasing stimulus concentrations affect both the amplitude and rise time of the calcium peak. These response parameters are plotted as a function of glutamate stimulus concentration in Fig. 5, *B* and *C*. The peak Ca^{2+} release increased nonlinearly with increasing stimulus intensity. At low glutamate concentrations, up to 10 nM, the Ca^{2+} change above basal was almost negligible. The magnitude of Ca^{2+} release increased rapidly in the 10- to 100-nM input range and then saturated at a peak ~1 μM Ca^{2+} at higher stimulus intensities. The inset of Fig. 5 *B* shows a plot for the peak $InsP_3$ response to the same stimulus protocol. The similarity between the stimulus function curves for peak Ca^{2+} and

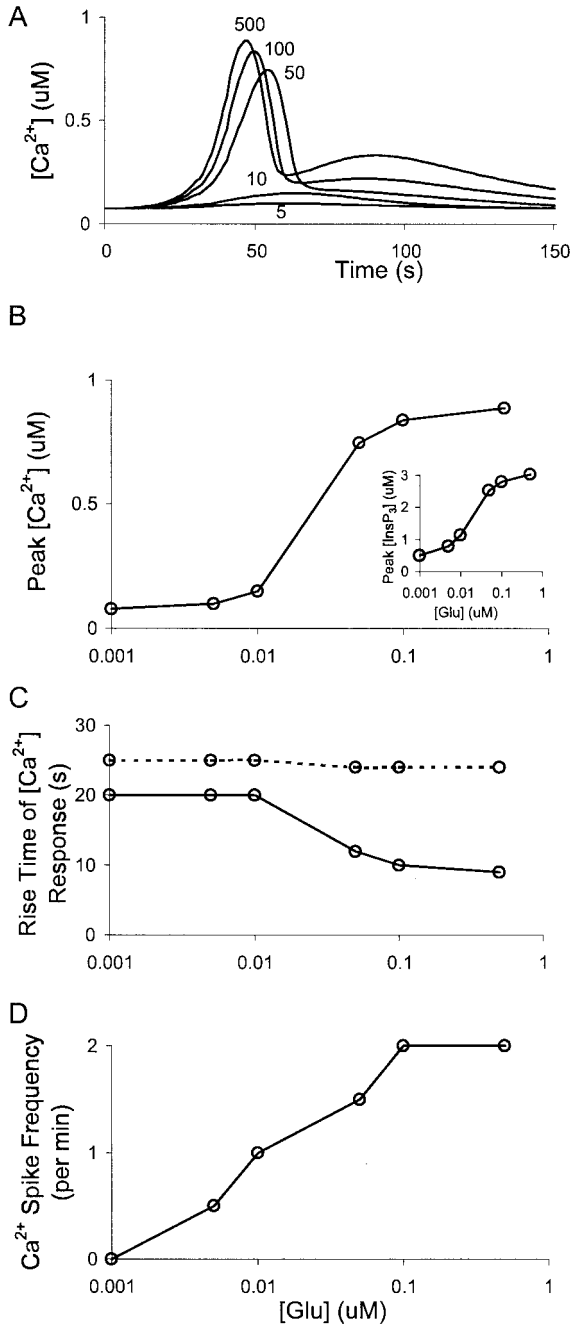

FIGURE 5 Ca^{2+} release as a function of intensity of glutamate stimulus. (*A*) Thirty-second pulses of 5 nM, 10 nM, 50 nM, 0.1 μM, and 0.5 μM glutamate are used as stimuli. The pulse amplitude in nanomolars is shown on the graph. For the non-Osc-model, rise time of the Ca^{2+} response decreases and amplitude increases with increasing stimulus intensity. (*B*) Peak Ca^{2+} responses (as obtained in *A*) are a nonlinear function of stimulus intensity. Inset shows a corresponding plot for the $InsP_3$ response. Glutamate concentrations (μM) represented on the *x* axis have a logarithmic scale. (*C*) Positive feedback of Ca^{2+} onto PLC β mediates the decrease in rise time of the Ca^{2+} response. The solid and dashed lines plot the rise time of the Ca^{2+} response as a function of stimulus intensity, in presence and absence of the positive feedback of Ca^{2+} onto PLC β, respectively. Stimulus protocol is same as that used for *A*. (*D*) Frequency of Ca^{2+} responses in the Osc-model are a nonlinear function of stimulus intensity. Stimuli used are 2-min pulses of 1 nM, 5 nM, 10 nM, 50 nM, 0.1 μM, and 0.5 μM glutamate, represented on a logarithmic scale on the *x* axis.

$InsP_3$ indicates that calcium release is a direct consequence of $InsP_3$ buildup. At higher concentrations of glutamate, there is higher occupancy of the mGluR, which leads to greater PLC β activation and buildup of more $InsP_3$. The plots show that there exists a relatively sharp stimulus threshold for $InsP_3$ generation and the subsequent Ca^{2+} release. In our model, this threshold is determined by the positive feedback of Ca^{2+} onto PLC β. PLC β has maximal activity when activated by both Gq and Ca^{2+}. In this form it catalyzes sufficient $InsP_3$ formation to elevate cytosolic Ca^{2+} levels over 10-fold above basal.

Fig. 5 *C* shows that the rise time of the Ca^{2+} response decreases with increasing stimulus intensity. This temporal acceleration of the peak response also results from the positive feedback of Ca^{2+} onto PLC β, which leads to regenerative calcium release. We tested this by removing the Ca^{2+} facilitation of PLC enzyme activity from our model. This resulted in an almost constant rise time of the Ca^{2+} response at any stimulus strength (Fig. 5 *C*).

We also performed simulations to study the effect of stimulus intensity on the Osc-model. Two-minute pulses of 1 nM, 5 nM, 10 nM, 50 nM, 0.1 μM, and 0.5 μM glutamate were used as stimuli. The frequency of calcium oscillations was taken as readout of the stimulus effect (Fig. 5 *D*) (Berridge, 1990). Like the calcium release in the non-Osc-model, the relationship between stimulus input and simulation output, oscillation frequency in this case, is nonlinear. A 1 nM glutamate stimulus produced no oscillations, whereas 0.1 and 0.5 μM stimuli produced a saturating response frequency of 2/min. The increase in frequency of oscillations is expected because increasing stimulus intensities produce increasing $InsP_3$ in the cytosol. At higher $InsP_3$ concentrations the bell-shaped conductance curve of the $InsP_3$ receptor with respect to calcium shows faster response kinetics than at lower concentrations (Fig. 3 *B*). This results in the greater number of calcium spikes within the same time period.

Effect of calcium oscillations on the $InsP_3$ metabolic cascade

It is known that the pattern of calcium oscillations regulates downstream events such as gene expression (Dolmetsch et al., 1998). Using our simulations we wanted to investigate whether oscillatory calcium dynamics also modify $InsP_3$ and other inositol phosphates by feedback. This is important as the different physiological functions of the various inositol phosphates could be temporally affected by the oscillations. For this purpose, the Osc-model was subjected to a stimulus pulse of 0.5 μM glutamate for 2 min. The calcium response generated by the pulse is represented in Fig. 6 *A*. Within stimulus time cytosolic calcium displayed oscilla-

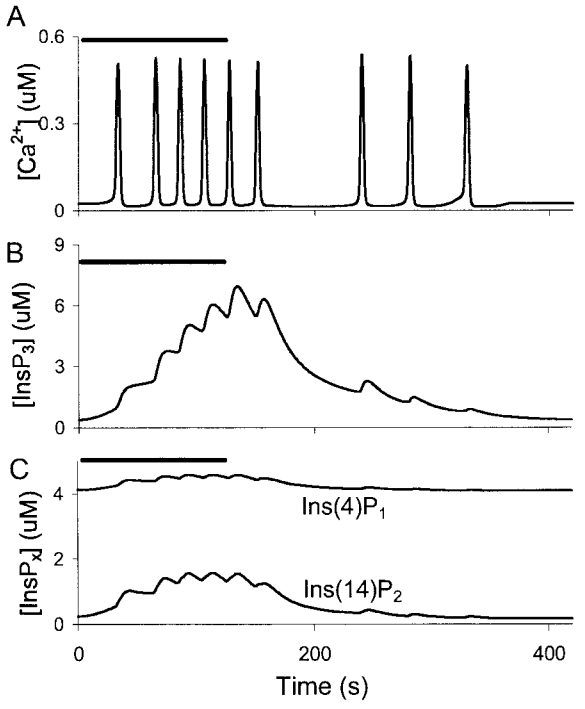

FIGURE 6 Responses of inositol phosphates in the Osc-model. Stimulus is a 2-min pulse of 0.5 μM glutamate (*solid bar*). (*A*) Oscillatory response of Ca^{2+}. Oscillations are of frequency ~2/min and persist beyond stimulus time. (*B*) $InsP_3$ levels oscillate in synchrony with Ca^{2+}. (*C*) Ins(1,4,5)P_3 oscillations are transmitted to its dephosphorylated products: Ins(1,4)P_2 and Ins(4)P_1, which also oscillate periodically with Ca^{2+}, but less prominently.

tions of uniform amplitude and similar interspike interval. Three residual Ca^{2+} spikes were also observed after stimulus termination, before $InsP_3$ was restored to basal levels. These residual spikes emerged after a time lag that represented the recovery time for the depleted ER calcium stores after the stimulus trigger. The 0.5 μM glutamate stimulus had emptied the stores to a level that Ca^{2+} could not be released until ER levels were adequately restored by the Ca^{2+}-ATPase pump.

Fig. 6, *B* and *C* depict the corresponding responses of Ins(1,4,5)P_3, Ins(1,4)P_2, and Ins(4)P_1 to the 2-min 0.5 μM glutamate pulse that generates the calcium response shown in Fig. 6 *A*. We observed that oscillatory calcium, which fed back onto PLC β-mediated $InsP_3$ generation, produced oscillations in $InsP_3$. We suggest that oscillations in cytosolic $InsP_3$ are possible, but instead of being a requirement for calcium release, they are generated as a result of feedback of calcium pulses. It has been shown experimentally that $InsP_3$ levels oscillate in cells (Hirose et al., 1999). At the same time, it has also been shown that nonoscillatory $InsP_3$ dynamics produce oscillations in calcium (Wakui et al., 1989). The Othmer-Tang model is also based on this formulation, wherein a square pulse of $InsP_3$ can generate pulsatile calcium release. Thus, our simulations, which combine the Othmer-Tang model with Ca^{2+} feedback onto $InsP_3$ generation, indicate that $InsP_3$ and calcium oscillations can coexist. However, it is not necessary that oscillations in calcium are brought about by oscillations in $InsP_3$.

Hirose et al. (1999) demonstrated that $InsP_3$ oscillates in a spatiotemporal manner in cells exhibiting calcium oscillations. These researchers showed a spatial component to the $InsP_3$ oscillations, wherein $InsP_3$ is translocated through the cytosol from its site of synthesis near the cell membrane to its site of action at the ER. They also discuss the role of a Ca^{2+}-mediated negative feedback in the generation of $InsP_3$ oscillations. As we have not incorporated any component in our model to account for spatial diffusion of $InsP_3$, we cannot comment on its spatial dynamics. We have also not included any negative feedback of calcium onto $InsP_3$ synthesis in our model.

The biochemical connections in the $InsP_3$ metabolic network transmit $InsP_3$ oscillations to its dephosphorylated metabolites (Fig. 6 *C*). Like $InsP_3$, the oscillations in Ins(1,4)P_2 and Ins(4)P_1 were also synchronous with calcium. Apart from Ins(1,4,5)P_3, Ins(1,4)P_2, and Ins(4)P_1, we observed negligible or no oscillatory perturbations for other inositol phosphates (not shown). This is expected from the response time courses of inositol phosphates downstream of $InsP_3$ phosphorylation (Fig. 2), which were so slow that oscillatory effects, if any, averaged out.

Hence, from our simulations we infer that the $InsP_3$ oscillations that we observe to be synchronous with calcium are a result of the competition between $InsP_3$ degradation and positive calcium feedback on $InsP_3$ synthesis.

Modification of Ins(1,4,5)P_3 response and calcium release by Ins(1,3,4,5)P_4

Research on the role of Ins(1,3,4,5)P_4 as a second messenger has over the years produced conflicting results. Recent evidence (Smith et al., 2000; Hermosura et al., 2000), however, supports the role of $InsP_4$ in facilitation of $InsP_3$-mediated calcium release. Whereas Smith et al. (2000) postulate that the function of $InsP_4$ is attributed to its possible control over ER membrane integrity, Hermosura et al. (2000) show that $InsP_4$ facilitation arises due to its metabolic effects. The latter view has also been supported in experiments on the *Xenopus* system (Sims and Allbritton, 1998). Both Ins(1,4,5)P_3 and Ins(1,3,4,5)P_4 share the same dephosphorylating enzyme: InsP 5-phosphatase. This enzyme converts Ins(1,4,5)P_3 to Ins(1,4)P_2 and Ins(1,3,4,5)P_4 to Ins(1,3,4)P_3. As $InsP_4$ competes with $InsP_3$ for the common enzyme, rapid $InsP_3$ degradation is inhibited. Thus, presence of $InsP_4$ results in a net gain in $InsP_3$ and hence in facilitation of calcium release.

Our biochemical model has the necessary components involved in interactions between $InsP_3$ metabolism and calcium release from stores. Hence, it was possible to simulate any effects that $InsP_4$ might have on calcium release. This is

also pertinent in context to our simulations as our model is based on parameters from brain tissue studies that report high expression levels of $InsP_3$ 3-kinase.

To understand the role of $InsP_4$, we made two modifications to our model that are represented in Fig. 7 *A*. Case (i) depicts the reaction scheme for the actual metabolism documented in literature. Here, Ins(1,4,5)P_3 is phosphorylated to Ins(1,3,4,5)P_4 by $InsP_3$ 3-kinase, and both $InsP_4$ and $InsP_3$ are dephosphorylated by the same InsP 5-phosphatase1. Case (ii) is a modification of the basic scheme where we uncouple $InsP_3$ and $InsP_4$ dephosphorylation. Here too $InsP_3$ is phosphorylated by $InsP_3$ 3-kinase, but only $InsP_3$ is dephosphorylated by $InsP_3$ 5-phosphatase1. In this scheme a separate enzyme, $InsP_4$ 5-phosphatase converts $InsP_4$ to Ins(1,3,4)P_3. The parameter values for these new phosphatases such as initial concentration and enzyme inhibition by inositol high polyphosphates are identical to those for InsP 5-phosphatase1 in the basic scheme. The K_m and V_{max} values of these phosphatases for their respective substrates match the corresponding enzyme activities that InsP 5-phosphatase1 exhibits toward $InsP_3$ and $InsP_4$ in the actual case.

In case (iii) we replace the entire network of $InsP_3$ metabolism with a single degradation step from $InsP_3$ to inositol. The degradation rate was set at 1.75/s, which produces the same basal turnover of $InsP_3$ as that in case (i) and (ii). The case (iii) model was used to characterize how $InsP_3$ and calcium dynamics change in a model that does not account for detailed $InsP_3$ metabolism. A comparison between the simulation outputs in case (ii) and (iii) can also suggest the importance of $InsP_4$ within the metabolic cascade. If model behavior upon uncoupling of $InsP_3$-$InsP_4$ dephosphorylation resembles the behavior upon complete deletion of the metabolic network, it would imply that $InsP_4$ represents the main effector of the entire network that determines the actual $InsP_3$ response.

Case (i), (ii), and (iii) models were made for both the non-Osc-model and the Osc-model. A 30-s 0.5 μM glutamate pulse was used to stimulate each of the three non-Osc-models (Fig. 7 *B*), and a 2-min pulse of similar amplitude was used for each of the Osc-models (Fig. 7 *C*). We find that $InsP_4$ indeed protects $InsP_3$ against hydrolysis. For the non-Osc-model and Osc-model, respectively, the peak $InsP_3$ response in the presence of the entire $InsP_3$ metabolic cascade was 1.8-fold and 3-fold greater than the response in the absence of either $InsP_3$-$InsP_4$ dephosphorylation coupling or detailed metabolism. The high degree of overlap of the $InsP_3$ responses for case (ii) and (iii) models suggests that in the amplitude domain, the influence of the detailed metabolism on $InsP_3$ dynamics is primarily mediated by Ins(1,3,4,5)P_4. Further for the non-Osc-model, the rise time for $InsP_3$ decreases by ~25% as a consequence of the protective role of $InsP_4$. Thus, our simulations predict that metabolic effects of $InsP_4$ modulate the temporal as well as the peak characteristics of the $InsP_3$ response.

Given the facilitation of $InsP_3$ buildup by $InsP_4$, we next wanted to analyze whether this translates into a greater mobilization of calcium. Because in our model we have not incorporated any direct influence of $InsP_4$ on any calcium channels, a facilitation observed in calcium release would imply a purely metabolic effect of $InsP_4$. Fig. 8 represents the calcium responses in the non-Osc-model and the Osc-

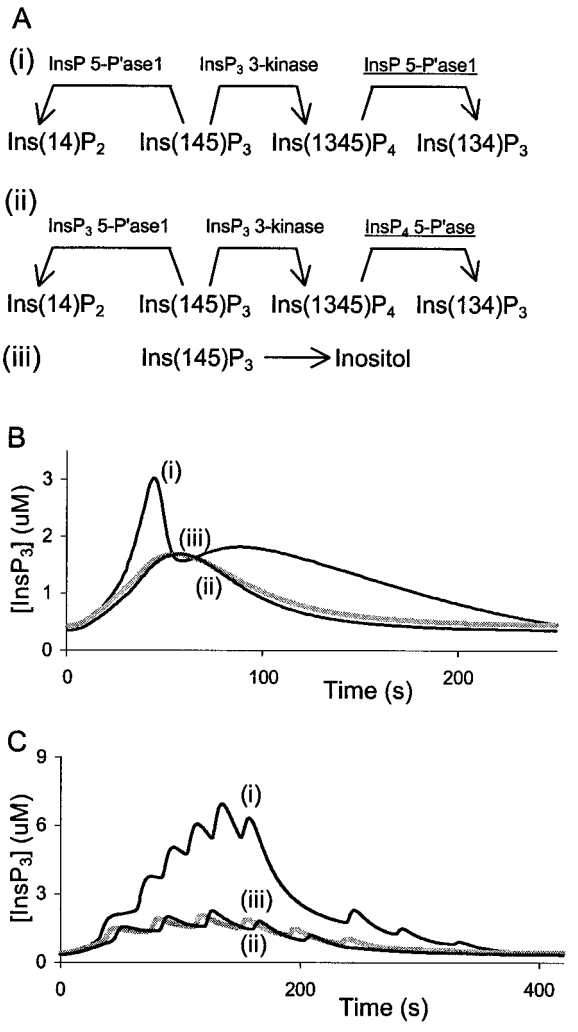

FIGURE 7 Ins(1,3,4,5)P_4 metabolically protects Ins(1,4,5)P_3 from degradation. (*A*) Schematic representation of modifications made to the model to analyze the metabolic function of Ins(1,3,4,5)P_4. (*i*) summarizes the actual metabolism documented in literature wherein both Ins(1,4,5)P_3 and Ins(1,3,4,5)P_4 are dephosphorylated by the same enzyme: inositol phosphate 5-phosphatase1. (*ii*) Represents a modification made to *i*, wherein Ins(1,4,5)P_3 is dephosphorylated by inositol trisphosphate 5-phosphatase1, and Ins(1,3,4,5)P_4 is dephosphorylated by inositol tetrakisphosphate 5-phosphatase. (*iii*) Represents a model wherein all details of $InsP_3$ metabolism have been replaced by a single step $InsP_3$ degradation to inositol. (*B*) Responses of $InsP_3$ for case *A* (*i*), *A* (*ii*), and *A* (*iii*) within the non-Osc-model. Stimulus used is a 30-s 0.5 μM pulse of glutamate. $InsP_3$ response for case (i) is 1.8-fold greater and rises 25% faster than responses in cases (ii) and (iii). (*C*) Responses of $InsP_3$ in case *A* (*i*), *A* (*ii*), and *A* (*iii*) within the Osc-model. Stimulus used is a 2-min 0.5 μM pulse of glutamate. $InsP_3$ response for case (i) is threefold greater than responses in cases (ii) and (iii). $InsP_3$ responses to case *A* (*iii*) in both the non-Osc-model and the Osc-model are represented as a gray line.

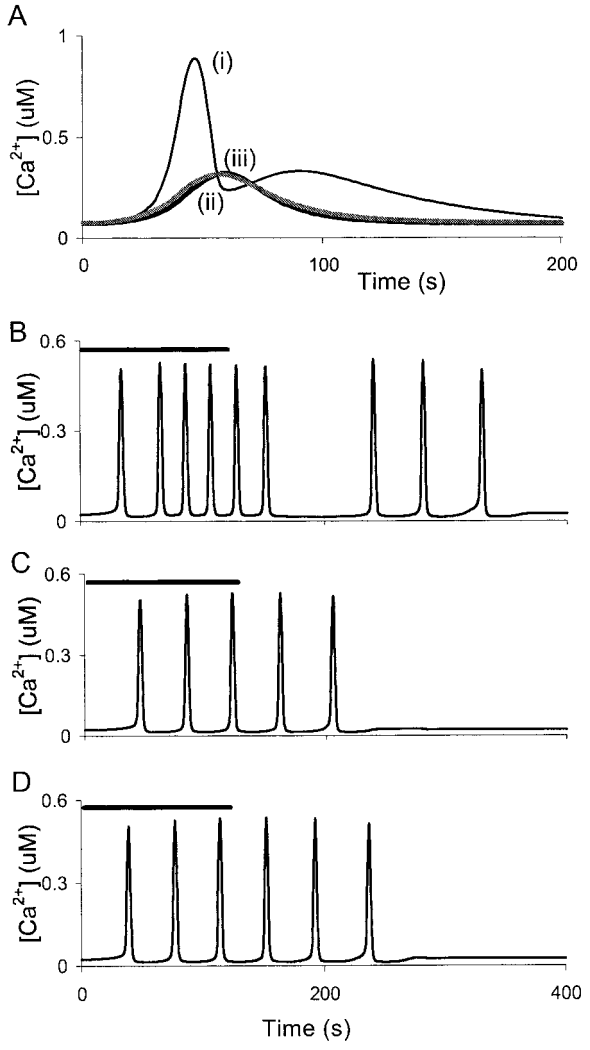

FIGURE 8 Ins(1,3,4,5)P_4 facilitates Ca^{2+} release via its metabolic effect. (*A*) Responses of Ca^{2+} to cases (i), (ii), and (iii) of Fig. 7 *A* within the non-Osc-model. Stimulus used is identical to that for Fig. 7 *B* (0.5 μM glutamate for 30-s). Ca^{2+} response for case (i) is threefold greater and rises 60% faster than response in cases (ii) and (iii). Ca^{2+} response to case *A* (*iii*) is represented as a gray line. (*B–D*) Responses of Ca^{2+} within the Osc-model to cases (i), (ii), and (iii) of Fig. 7 *A*, respectively. Stimulus used in *B, C,* and *D* is identical to that for Fig. 7 *C*, 0.5 μM glutamate for 2-min (*solid bars*). Frequency of Ca^{2+} oscillations is modulated by $InsP_4$. An oscillation frequency of 2/min in *B* is reduced to 1.5/min in *C* and *D*.

model, that correspond to the $InsP_3$ responses shown in Fig. 7, *B* and *C*. Responses within the non-Osc-model (Fig. 8 *A*) show that $InsP_4$ also facilitates the calcium release response via its positive effect on $InsP_3$. The peak calcium release in the presence of the intact metabolic network was approximately threefold the calcium response in the absence of enzyme competition between $InsP_4$ and $InsP_3$. Moreover, the shape of the Ca^{2+} response also changed from a biphasic curve to a bell-shape in the modified versions of the reference model. The rise time for calcium in case (i) was ~60% smaller than that in case (ii) and (iii). Thus, both the increase in amplitude and the decrease in rise time for calcium were greater than those observed for the $InsP_3$ response (Fig. 7 *B*) in the non-Osc-model. This suggests that the magnitude of $InsP_4$ facilitation is greater for $InsP_3$-mediated Ca^{2+} release than for the metabolic response of $InsP_3$.

We also noted that the temporal responses of $InsP_3$ and Ca^{2+} upon $InsP_3$-$InsP_4$ dephosphorylation uncoupling were almost identical to their behavior upon complete deletion of the metabolic network (Fig. 7 *B* and 8 *A*). This implies that $InsP_4$ is the principal effector of the inositol phosphate cascade that modulates $InsP_3$ and, subsequently, Ca^{2+}. $InsP_4$ kinetics are mainly governed by its synthesis via $InsP_3$ 3-kinase. The CaM and CaMKII activated forms of this enzyme have reversible kinetics in our model. If these enzyme activities are modeled using the Michaelis-Menten formulation, responses for case (ii) and (iii) model modifications differ markedly (not shown). For the irreversible enzyme scheme, the large influence of the first order network interaction with $InsP_4$ on $InsP_3/Ca^{2+}$ is reduced, and secondary network interactions become necessary to explain their responses. However, because reversible enzyme kinetics are a more accurate representation of metabolic flow in this case, we suggest that behavior of $InsP_3/Ca^{2+}$ is governed by the metabolic network mainly at the first rather than higher order interaction level.

Recent experiments (Zhu et al., 2000) show that Ins(1,3,4,5)P_4 can function as a frequency regulator of calcium oscillations in cells. Inhibition of $InsP_3$ 3-kinase can significantly reduce the oscillation frequency or abolish calcium oscillations, depending on the degree of enzyme inhibition. We also analyzed the effects of $InsP_4$ on calcium oscillations within our Osc-model. Fig. 8, *B*, *C*, and *D* represent the oscillatory calcium responses that correspond to the case (i), (ii), and (iii) time curves of $InsP_3$ in Fig. 7 *C*. The calcium curves show no modulation of amplitude but marked temporal differences. The ineffectiveness of $InsP_4$ in mediating a change in peak calcium is not surprising. Maximal calcium released per spike is tightly regulated by positive and negative feedback of calcium onto the $InsP_3$ receptor. Only drastic alterations in the cytosolic or ER calcium buffering would be expected to vary the peak height of calcium per oscillation. At the same time, the frequency modulating effect of $InsP_4$ can also be explained. Fig. 7 *C* shows that the peak $InsP_3$ response for case (i) is threefold greater than the response when $InsP_3$-$InsP_4$ metabolism is decoupled. A higher $InsP_3$ buildup corresponds to faster response kinetics of the $InsP_3$ receptor (Fig. 3 *B*). Thus, higher $InsP_3$ levels generate more frequent calcium spikes within the same time than lower $InsP_3$ levels. Our simulations also display this phenomenon. The intact $InsP_3$ metabolism model with coupled $InsP_3$-$InsP_4$ dephosphorylation shows maximal oscillation frequency of 2/min (Fig. 8 *B*). On the other hand, the frequency drops to 1.5/min for both case (ii) and (iii) in which $InsP_4$ does not protect $InsP_3$ from hydrolysis (Fig. 8, *C* and *D*). Our model does not

include any direct Ca^{2+} mobilizing effects of $InsP_4$. Thus, we suggest that the metabolic function of $InsP_4$ to protect $InsP_3$ from hydrolysis is sufficient to generate higher frequency oscillations of calcium.

Function of $InsP_4$ as a "coincidence detector"

Natural stimulus inputs are often composed of repetitive pulse patterns. It adds to the response capabilities of a cellular system if it can detect stimuli spaced in time, apart from stimuli of different intensities. It has been suggested that $InsP_4$ may function as a "coincidence detector" for the $InsP_3$ signaling pathway (Irvine, 2001; Parker and Ivorra, 1991). This means that an otherwise subthreshold stimulus can generate a calcium response if it is coincident with presence of some $InsP_4$ that has remained in the system from a similar previous stimulation. Hermosura et al. (2000) performed a key experiment to demonstrate this phenomenon. They used a paired pulse stimulus protocol wherein the GPCR agonist concentration used was below the threshold for any measurable calcium release. When the second pulse of agonist followed the first pulse within a particular time frame, an intracellular calcium signal was detected. Such facilitation was not seen when the $InsP_3$ 3-kinase was pharmacologically blocked.

We investigated whether our Osc-model, which has a more accurate representation of $InsP_3$ receptor kinetics than the non-Osc-model, can produce facilitation of paired subthreshold stimuli. As shown in Fig. 9, our pulse protocol consisted of an initial 20 nM glutamate pulse for 20-s followed by a second identical pulse after 90, 100, 110, 120, or 130 s. A single 20-nM glutamate pulse of 20-s duration, is incapable of generating a calcium spike. If the second 20-nM pulse succeeds the first within 90 s, a calcium response is always generated. This is because the subthreshold levels of $InsP_3$ generated in the system by the two stimuli sum to become suprathreshold and release calcium. After 90 s of the first stimulus, $InsP_3$ levels have significantly reduced. At this time however, $InsP_4$ levels remain in the system due to its slower degradation than $InsP_3$ (Fig. 2). If the 20 nM glutamate pulse is now given, this residual $InsP_4$ can perform its metabolic function to protect any new $InsP_3$ from degradation. The higher levels of $InsP_3$ generated during the second pulse would then result in calcium release. Fig. 9 *A* shows such an effect, wherein the four calcium spikes displayed correspond to stimulus interpulse intervals of 90, 100, 110, and 120 s, respectively. The corresponding response of $InsP_3$ shows that its levels are potentiated during the second glutamate stimulus (Fig. 9 *B*). No calcium release is seen for the last stimulus protocol with a pulse spacing of 130 s. By this time, residual $InsP_4$ from the first stimulus has degraded below the threshold level at which it can protect new $InsP_3$ from fast hydrolysis. We further confirmed that the paired pulse facilitation was due to the metabolic function of residual $InsP_4$ during the second pulse, and not simply due to summing of $InsP_3$ responses across temporally close stimuli. For this, we subjected our version of the Osc-model with decoupled $InsP_3$-$InsP_4$ metabolism (Fig. 7 *A*, case (ii)) to the same stimulus protocol as described above. This model did not

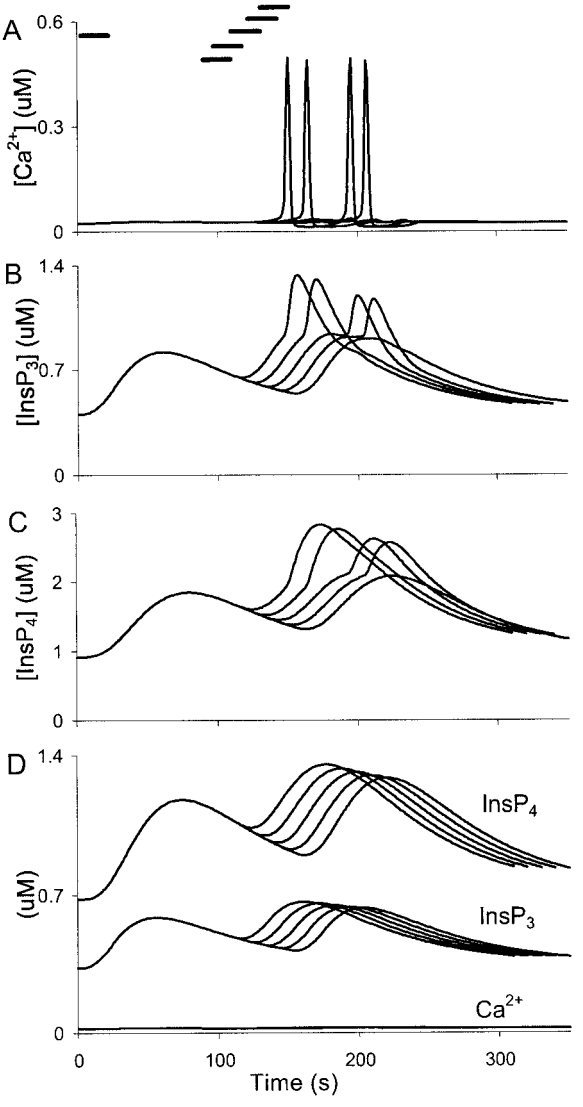

FIGURE 9 Protective role of $InsP_4$ leads to paired pulse facilitation. All stimulus pulses (*solid bars*) are of 20 nM glutamate delivered for 20-s. Pulse 1 initiates at 0 time. Pulse 2, shown as solid bars in a ladder arrangement in *A*, follows pulse 1 after 90, 100, 110, 120, or 130 s. (*A–C*) Responses of Ca^{2+}, $InsP_3$, and $InsP_4$, respectively, to the paired pulse protocols. The four Ca^{2+} spikes in *A* correspond to delivery of pulse 2 after 90, 100, 110, or 120 s, respectively. An interpulse interval of 130 s does not generate any Ca^{2+} response. Interpulse intervals less than 90 s (not shown here) produce multiple Ca^{2+} spikes as residual $InsP_3$ from pulse 1 summates with the new $InsP_3$ from pulse 2. Beyond 90 s, $InsP_3$ from pulse 1 has significantly diminished and Ca^{2+} release effects during pulse 2 are attributed to $InsP_4$. (*D*) Response of the Osc-model that has decoupled $InsP_3$-$InsP_4$ dephosphorylation to the same paired pulse protocol. The Ca^{2+}, $InsP_3$, and $InsP_4$ responses are labeled. No Ca^{2+} response is induced in this model.

show any calcium spiking for the paired stimuli (Fig. 9 *D*). Our simulations thus show that $InsP_4$ can serve as a short lived "memory" for a previous exposure of a system to an $InsP_3$ generating stimulus.

It is also interesting to note that during the second stimulation, $InsP_4$ indirectly also facilitates its own levels (Fig. 9 *C*). Such an effect could also be important for calcium release kinetics if $InsP_4$ has a direct action on any calcium channel, such as the $InsP_3$ receptor (Hermosura et al., 2000).

Effects of high inositol polyphosphates on inositol phosphate metabolism

We wanted to analyze how a significant perturbation in the inositol high polyphosphates affects the dynamics of the metabolic network. Stimulation of IHPs does occur in cells especially during the S phase of the cell cycle, but this does not require activation of PLC β or generation of Ins(1,4,5)P_3 (Balla et al., 1994). Our simulations have also shown that a stimulus pulse that first generates Ins(1,4,5)P_3 and subsequently activates other components of the inositol phosphate metabolic network, does not propagate upto the IHPs (Fig. 2). Thus, to study effects of elevation in IHP levels we applied direct stimulation to the system in the form of a 30-s pulse of 100 μM $InsP_5$ (twice its original concentration).

The most striking differences between stimulation via $InsP_5$ and $InsP_3$ lay in the temporal domain. The time taken by the whole system to regain steady-state post-$InsP_5$-stimulation was ~2.5 h compared with 10 to 15 min required after $InsP_3$ stimulation. $InsP_5$ and $InsP_6$ have very large cellular pools and slow metabolism kinetics. Hence, they take a long time to equilibrate, and in turn the entire system does not attain steady state for over 2 h. However, given that the IHPs are so important for cell biological processes, direct regulatory mechanisms must exist to modulate their responses and to hasten their equilibration. Some reports suggest that cell cycle factors may regulate the IHP responses (Balla et al., 1994; Guse et al., 1993). Our model could not incorporate any regulation of IHPs reported in literature, as their exact molecular details are not characterized. Nevertheless, it is clear that such regulation would play an important role in the temporal dynamics of stimulated IHPs.

At equilibrium $InsP_5$ is dephosphorylated to both Ins(1,4,5,6)P_4 and Ins(3,4,5,6)P_4, generating approximately equivalent levels of each. Upon $InsP_5$ stimulation we observed a ~30-fold elevation in Ins(3,4,5,6)P_4 levels and an approximately twofold change for Ins(1,4,5,6)P_4 (Fig. 10, *A* and *C*). The greater stimulation of Ins(3,4,5,6)P_4 than Ins(1,4,5,6)P_4 was due to the faster rate of $InsP_5$ 1-phosphatase compared with $InsP_5$ 3-phosphatase in our model. Despite this, both $InsP_4$ responses were much larger than for $InsP_3$-mediated stimulation. Ins(1,3,4,5)P_4 and Ins(1,3,4,6)P_4 were also stimulated by approximately twofold. However, the Ins(1,3,4,5)P_4 response was insignificant compared with its 60-fold stimulation via the PLC β route, as $InsP_5$ did not trigger $InsP_3$ 3-kinase activation via Ca^{2+} release.

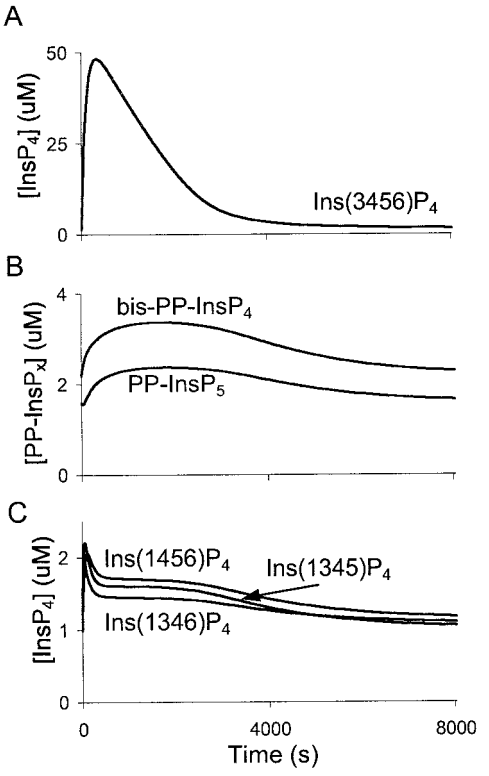

FIGURE 10 Responses of inositol phosphates to a 30-s stimulus of 100 μM $InsP_5$. Time on the *x* axis represents 2.2 h of simulation run (post-stimulation). (*A*) Ins(3,4,5,6)P_4 undergoes the largest fold response. (*B*) Responses of inositol pyrophosphates: PP-$InsP_5$ and bis-PP-$InsP_4$ are slow and ~1.5-fold in magnitude. (*C*) Inositol tetrakisphosphates: Ins(1,4,5,6)P_4, Ins(1,3,4,5)P_4, and Ins(1,3,4,6)P_4 have ~twofold responses that recover quickly from the perturbation.

Stimulation of inositol pyrophosphates, PP-$InsP_5$, and bis-PP-$InsP_4$ was ~1.5-fold (Fig. 10 *B*). Such minimal activation perhaps implies that these molecules have further distinct stimulatory mechanisms. Indeed, Safrany and Shears (1998) have shown that turnover of bis-PP-$InsP_4$ is specifically regulated by β_2-adrenergic receptors through a cAMP-mediated mechanism. From Fig. 10, it was also evident that $InsP_4$s that have direct interaction with the lower inositol phosphates have faster time responses to $InsP_5$ stimulation than molecules isolated within the IHP pool, which equilibrate slowly.

The lower phosphates from $InsP_3$ down were negligibly affected by the 100 μM $InsP_5$ pulse (not shown). The buildup of these inositol bisphosphates and monophosphates was hampered because $InsP_5$ and $InsP_6$ directly inhibit the enzymes that synthesize them, specifically InsP 5-phosphatase1 and InsP 4-phosphatase. It was earlier observed from the $InsP_3$-mediated stimulation (Fig. 2) that the IHPs probably form a separate biochemical pool, which is unaffected by the lower phosphates. Stimulation via $InsP_5$

reveals that large perturbations in the higher phosphate pool are biochemically networked to the lower phosphate pool in such a way that the lower phosphates remain at basal levels. Thus, we conclude that the inositol high and low polyphosphate pools are indeed distinct and fail to generate fluctuations in each other when independently stimulated.

Sensitivity analysis of the $InsP_3$ metabolism model

The model that we have built uses parameter constraints from biochemical test-tube experiments that estimate cellular concentrations and characteristic K_m and V_{max} values of enzymes. These may not necessarily mimic the in vivo environment and may vary depending on the sensitivity of the experimental technique used for the analyses. In such a situation it is useful to test the robustness of our model by subjecting every parameter used to graded alterations spanning a wide range. This gives an idea of the performance of the model across changes within the system. Further, the outliers emerging from such an analysis suggest the regulatory inputs in our model to which the simulations are extremely sensitive.

We scaled all parameters used in our model from one-tenth to 10-fold their original value (see Materials and Methods). Three sample sensitivity plots are shown in Fig. 11. In Fig. 11 *A*, changes in $InsP_3$ output are taken as readout of the sensitivity analysis performed on all reaction steps used in the model. K_d was the parameter being altered. As expected, major changes in $InsP_3$ resulted from changes in the K_d of reactions directly involved in its synthesis. These include activation of G protein by glutamate binding to its receptor (Activate-Gq), basal activation of G-protein (Basal-Act-G), activation of PLC β by Gα-GTP binding (Act-PLC-by-Gq), and the composite basal rate of PIP_2 hydrolysis due to other PLCs in the system (basal). It was observed that $InsP_3$ was less sensitive to changes within the metabolic cascade.

The log scatter plot in Fig. 11 *B* represents variations in the calcium output as a result of perturbations in the V_{max} of all enzymes used in our model. Calcium release critically depended on calcium feedback onto PLC β (PLCb-Ca-Gq) and also on metabolism of $InsP_3$. Simulations showed sensitivity toward both the $InsP_3$ 5-phosphatase isoforms that dephosphorylate $InsP_3$ to Ins(1,4)P_2 (ip3_5pase1, ip3_5pase2), as well as to the activated $InsP_3$ 3-kinase that converts $InsP_3$ to Ins(1,3,4,5)P_4 (ip3-3k*). It was interesting to note that calcium output was also sensitive to V_{max} for the Ins(3,4,5,6)P_4 1-kinase enzyme activity (ip4-1k-off) that phosphorylates Ins(3,4,5,6)P_4 to $InsP_5$. On stimulation, this reversible enzyme functions such that accumulation of its substrate, Ins(3,4,5,6)P_4 is significant. Elevation in $InsP_4$ levels inhibits calcium stimulated chloride efflux across the plasma membrane. If $InsP_4$ 1-kinase also affects calcium levels, then an indirect means of inhibition of the calcium-driven chloride channel (apart from direct binding of $InsP_4$ to the channel) may exist. Ca^{2+} release was also sensitive to the rate of calcium efflux to the extracellular space (Ca-pump-out).

Fig. 11 *C* shows a sensitivity analysis performed on the Osc-model. Alterations made to the initial concentrations of kinetic pools are monitored using the frequency of oscillations as readout of the output. We observed that Ca^{2+} oscillations were directly affected by the concentration of kinetic pools that determine receptor-based PLC β activation, such as the metabotropic glutamate receptor (mGluR), PIP_2, G-protein (G-GDP), and PLC β. Sensitivity was also seen toward pools that determine equilibration of cytosolic calcium with ER and extracellular calcium, such as leak across the ER membrane (ER_leak), ER-Ca^{2+}-ATPase pump (ER_pump), calcium extracellular efflux pump (Ca-EPump), $InsP_3$ receptor (IP3R), and the calcium buffer capacity of the ER (Calsequestrin). We note that sensitivity of the nonoscillatory calcium response toward most of these Ca^{2+} equilibration-determining pools was small. This was expected because generation of calcium oscillations requires a very tight combination of all parameters that determine calcium levels. Tenfold changes in these parameters can completely abolish oscillations. Within the metabolic cascade Ca^{2+} oscillations were most sensitive to the two isoforms of $InsP_3$ 5-phosphatase (IP 5pase1, IP3 5pase2) and $InsP_3$3-kinase (IP3 3K). As seen earlier, these same enzymes were also the key modulators of the nonoscillating calcium output.

Additional sensitivity analysis plots for single parameter variations are presented in Supplementary Information. In these analyses also, the sensitive parameters were same as those summarized above, implying that the sensitive subset of the total parameter space remains constant across different analyses. Further, we found that for enzyme-based parameters, the sensitive subset is independent of mechanistic details for the enzymes, i.e., whether they have been modeled as per the reversible scheme or the Michaelis-Menten scheme.

We also performed two global sensitivity analyses (not shown) to assess the effects of simultaneous variations in a combination of parameters on our model (see Materials and Methods). For the non-Osc-model, rate scaling for all enzymes and reactions as a function of 10°C rise in temperature resulted in ~60% positive change in response peaks of Ins(1,4,5)P_3 and Ins(1,3,4,5)P_4, whereas a 10°C temperature drop led to ~30% negative change in their outputs. Peak Ca^{2+} release was more tolerant to the temperature variation with a ~30% to 40% change for the ±10°C shift, although its basal levels were influenced twofold. Ins(1,3,4)P_3 was found to be much less sensitive to temperature effects. The temperature-based perturbation also shifted response latencies for the network components by 30 to 60 s. The Osc-model was less robust to temperature perturbations and could maintain the control oscillatory response only within a ±2.5°C temperature range. Oscillations were found to become more frequent and dampen at lower temperatures.

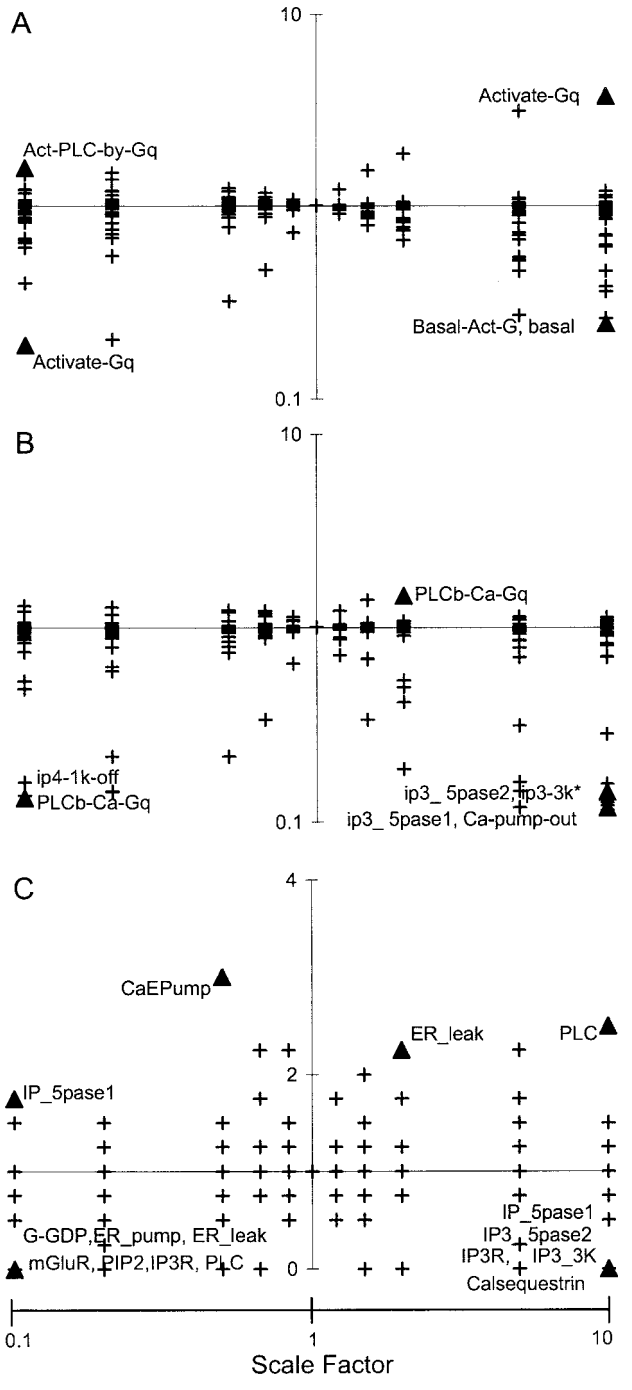

FIGURE 11 Scatter plots for sensitivity analysis of the $InsP_3$ metabolism model. (*A* and *B*) Represents the non-Osc-model; (*C*) represents the Osc-model. Both axes have logarithmic scales, except in *C* where only the *x* axis is logarithmic. The *x* axis represents the scale factor by which a parameter is altered with boundaries of 0.1 and 10 times the original value of the parameter. The *y* axis represents the normalized fold change in output due to the parameter scaling. Outliers in the scatter plots correspond to the parameters to which the simulations are very sensitive. Some of the most significant outliers have been marked with solid triangles and labeled alongside. Multiple parameter labels beside a solid triangle imply that the output is equally sensitive to all these parameters. (*A*) Normalized fold changes in $Ins(1,4,5)P_3$ output as a function of reaction K_d scaling. (*B*) Normalized fold changes in Ca^{2+} output as a function of enzyme V_{max} scaling. (*C*) Normalized changes in the frequency of Ca^{2+} oscillations as a function of initial concentration scaling.

The second global sensitivity analysis based on ATP depletion showed $InsP_4$ and Ca^{2+} to be most sensitive to the 85% drop in ATP levels, for which their peak stimulated levels dropped by 80% and 75%, respectively. Once again, the Osc-model was more sensitive to this global perturbation. Oscillations became more frequent and dampened at 50% ATP levels and disappeared for the 85% ATP depletion where basal cytosolic Ca^{2+} had increased 1.5-fold.

These global analyses thus show that our model is fairly robust to physiologically expected system alterations. Single parameter variation analyses lead us to conclude that the model is sensitive to a defined set of parameters that are a small subset of the entire parameter space. Interestingly, these same parameters have been extensively studied experimentally due to their significant influence on our network of interest (Zhu et al., 2000; Hermosura et al., 2000; Albrecht et al., 2002). Thus, despite the limitation that our model is based on a large parameter space (Table 2), which itself has certain degree of error attached to it arising from experiments, we suggest that our results do reflect characteristics of the biological system.

DISCUSSION

We have built a mass action kinetic model for the inositol phosphate metabolic network. This model accounts for most interactions among inositol phosphates ranging from $InsP_1$ isoforms to the $InsP_8$ equivalent bis-PP-$InsP_4$ that have been biochemically characterized and reported in literature. Further, our model couples the $InsP_3$ metabolic cascade with the synthesis of $InsP_3$ via G-protein coupled metabotropic glutamate receptor-driven PLC β activation and with the function of $InsP_3$, i.e., release of Ca^{2+} from intracellular Ca^{2+} stores. Using varied glutamate stimulus protocols at the mGluR, we have studied the cross-talk among the members of the inositol phosphate network. By comparing and contrasting the stimulus response outputs, we suggest interpretations as to how the network components influence and modulate each other. We have also investigated how the metabolism of $InsP_3$ affects its calcium release function. We report three major results of our simulations. 1) In our model Ca^{2+} released through the $InsP_3$ receptor feeds back onto PLC β to regenerate $InsP_3$ and hence mobilize more Ca^{2+}. Thus dynamics of the Ca^{2+} waveform in turn influence the response pattern of the various inositol phosphates that branch out from $InsP_3$. We have also incorporated detailed kinetics of the $InsP_3$ receptor, which produce cytosolic Ca^{2+} oscillations to study fine aspects of interactions between Ca^{2+} and inositol phosphate derivatives. 2) In our simulations $Ins(1,3,4,5)P_4$ emerges as an important modu-

lator of the temporal dynamics of other inositol phosphates. We also show that Ins(1,3,4,5)P_4 facilitates Ca^{2+} release with respect to both the timing and peak of the Ca^{2+} response. 3) Our simulations further demonstrate that $InsP_4$ serves as a coincidence detector for paired subthreshold stimuli, and enables Ca^{2+} release in situations where it would not have otherwise been possible.

Interactions within the inositol phosphate metabolic network

The current simulations highlight an important property of the elaborate interlinking within the metabolic network. This is that if flux of one of the components becomes dominant over others, that particular metabolite can modulate downstream enzyme activities beyond the primary and secondary interaction level. Ins(1,3,4,5)P_4 undergoes up to 60-fold stimulation in our model because of both the high expression levels of its synthesizing enzyme $InsP_3$ 3-kinase as well as its strong positive regulation by Ca^{2+}-CaM and CaMKII. We observe that under the influence of this $InsP_4$, inositol phosphates downstream of it, i.e., Ins(1,3,4)P_3 and its dephosphorylated forms exhibit rectangular waveforms. These inositol phosphates "freeze" at their respective peaks as long as $InsP_4$ levels are elevated and their synthesizing enzymes are substrate-saturated. Interestingly, the Ins(1,3,4)P_3 waveform propagates through the network such that temporal response of Ins(3,4,5,6)P_4 also has a long elevated plateau phase. Such prolonged elevation can provide these molecules with a relatively long-term capacity for cellular function, which endures even after the stimulus is removed. This is in sharp contrast to the transient spike of Ins(1,4,5)P_3, which is transduced to a Ca^{2+} signal within stimulus time.

We also show that Ins(1,3,4,5)P_4 not only affects inositol phosphates downstream of it, but also influences Ins(1,4,5)P_3. This is attributed to the unique property of InsP 5-phosphatase1 to dephosphorylate both Ins(1,4,5)P_3 and Ins(1,3,4,5)P_4. In its competition for the same enzyme, $InsP_4$ ends up slowing $InsP_3$ hydrolysis and enhancing its buildup. Indeed, when we decouple the two enzyme activities of the 5-phosphatase, we see that not only is the peak $InsP_3$ response diminished, but its rise time is also delayed.

With respect to the inositol high polyphosphates, consistent with experimental findings, our simulations show negligible effects of a GPCR stimulus. It has been suggested that the IHPs are a biochemical pool separate from the lower phosphates and are uniquely modulated by other cellular mechanisms. Our investigation of the effects of direct IHP stimulation unexpectedly showed negligible perturbations in the lower phosphates. Careful examination of the model revealed that IHPs are networked such that they directly inhibit the enzymes that synthesize the lower phosphates. Thus, when independently stimulated, neither higher phosphates nor lower phosphates can perturb each other. Higher phosphates function as regulators of vesicle trafficking, whereas lower phosphates are directly or indirectly involved in gating ion channels such as the $InsP_3$ receptor. The segregation of their metabolic flux pools within the inositol phosphate network may be important for the temporal control of their discrete functions.

Interactions between $InsP_3$ metabolism and calcium release

In our model, $InsP_3$ metabolism and Ca^{2+} release from the ER have both feed forward and feed backward links. Metabolites of $InsP_3$ such as Ins(1,3,4,5)P_4 can influence Ca^{2+} by modifying $InsP_3$ dynamics. Ca^{2+}, on the other hand, can affect inositol phosphates via $InsP_3$ regeneration through PLC β feedback activation or CaM/CaMKII-mediated $InsP_3$ 3-kinase activation or InsP 1-phosphatase inhibition. We have explored the possible outcomes of such interactions in our model. We show that positive feedback of Ca^{2+} onto PLC β is critical for the Ca^{2+} release function. Without this, stronger stimulation of the system does not result in a greater amount of Ca^{2+} release or a faster response. Further, when Ca^{2+} dynamics are oscillatory, this positive feedback to $InsP_3$ generation competes with $InsP_3$ degradation to bring about oscillations in $InsP_3$ and its lower phosphate derivatives. Thus, even though we did not include oscillations in $InsP_3$ as a prerequisite for Ca^{2+} oscillations in our model, we observe $InsP_3$ oscillations as a result of the Ca^{2+} feedback. We propose that in cells both $InsP_3$ and Ca^{2+} oscillations may coexist, but it is not necessary that oscillations in Ca^{2+} depend on oscillation in $InsP_3$.

How does the metabolic cascade influence Ca^{2+} dynamics? We find that the metabolic coupling of Ins(1,4,5)P_3 to Ins(1,3,4,5)P_4 via InsP 5-phosphatase1 increases the responsiveness of Ca^{2+} to stimuli. The peak Ca^{2+} response is reduced, and its rise time is prolonged in absence of the dual substrate specificity of the InsP 5-phosphatase for $InsP_3$ and $InsP_4$. This modification also diminishes the frequency of Ca^{2+} oscillations. Experimentally it has been demonstrated that the facilitatory function of $InsP_4$ is abolished if $InsP_3$ 3-kinase, which synthesizes Ins(1,3,4,5)P_4, is pharmacologically inhibited (Hermosura et al., 2000). As this strategy completely blocks generation of Ins(1,3,4,5)P_4, it would also drastically influence all inositol phosphates downstream of it. This can further adversely affect the various cellular functions regulated by these inositol phosphates. Our simulation strategy to replace the common 5-phosphatase for $InsP_3$ and $InsP_4$ by two separate enzyme activities, exclusively affects Ins(1,3,4,5)P_4 and not any other component of the metabolic network. Even though such enzyme modification highlights $InsP_4$ function more clearly, it may be technically difficult to emulate in experiments. Further, we find Ca^{2+} release upon complete exclusion of the metabolic network linked to $InsP_3$ in our model to be equivalent to that upon $InsP_3$-$InsP_4$ uncoupling. This equivalence emerges only when activated $InsP_3$

3-kinase is modeled appropriately as a reversible enzyme. Thus, accounting for non-Michaelis-Menten enzyme kinetics in our model allows us to propose that only primary level interactions within the metabolic cascade, i.e., $InsP_3$ to $InsP_4$, may be responsible for potentiation of the $InsP_3$-mediated Ca^{2+} response.

Finally, we show that our system can exploit the inositol phosphate networking to broaden its response repertoire to GPCR stimuli. If any remnants of $Ins(1,3,4,5)P_4$ from a brief stimulation persist till a second stimulus arrives, a Ca^{2+} response is generated even if the stimuli are subthreshold for Ca^{2+} release. This directly stems from the "protective" function of $InsP_4$ that can modify $InsP_3$ dynamics from one stimulus to another.

Thus, we conclude that interactions between metabolism of $InsP_3$ and Ca^{2+} release are important for this signaling cascade to process diverse patterns of stimuli.

Interpretations and limitations

We are aware that the current simulations are an approximation to the actual biology of the system. One of the major limitations of this mass action model is that it relies on test-tube experiments that are not an accurate reflection of in vivo interactions. These experiments cannot mimic intracellular environments that are subject to modifications by various cellular features such as cystoskeletal elements, membrane localization, and organelle compartmentalization. Further, the biochemical parameters may significantly change over the years as the technology for experimentation improves.

Despite these limitations, our model replicates known physiological properties of inositol phosphates reasonably well. Point mass action kinetics may be a good first approximation because $InsP_3$ and its derivatives are likely to diffuse through most of the cell on the time scales of interest. Further, the sensitivity analysis of our simulations suggests that our model is quite robust across parameter variations that have arisen in literature due to different technical approaches to the same experiments. Thus, our model and its predictions concerning inositol phosphate dynamics and their interactions with $InsP_3$-mediated Ca^{2+} release may be a useful step toward understanding of the fundamental properties of this complex metabolic network.

J.M. is supported on a NCBS/TIFR fellowship. U.S.B. is a Senior Research Fellow of the Wellcome Trust. We thank Dr. S. B. Shears for advice on parameter values.

REFERENCES

Albrecht, M. A., S. L. Colegrove, and D. D. Friel. 2002. Differential regulation of ER Ca^{2+} uptake and release rates accounts for multiple modes of Ca^{2+}-induced Ca^{2+} release. *J. Gen. Physiol.* 119:211–233.

Balla, T., S. S. Sim, A. J. Baukal, S. G. Rhee, and K. J. Catt. 1994. Inositol polyphosphates are not increased by overexpression of $Ins(1,4,5)P_3$ 3-kinase but show cell-cycle dependent changes in growth factor-stimulated fibroblasts. *Mol. Biol. Cell.* 5:17–27.

Bansal, V. S., R. C. Inhorn, and P. W. Majerus. 1987. The metabolism of inositol 1,3,4-trisphosphate to inositol 1,3-bisphosphate. *J. Biol. Chem.* 262:9444–9447.

Batty, I. H., A. J. Letcher, and S. R. Nahorski. 1989. Accumulation of inositol polyphosphate isomers in agonist-stimulated cerebral-cortex slices: comparison with metabolic profiles in cell-free preparations. *Biochem. J.* 258:23–32.

Berridge, M. J. 1990. Calcium oscillations. *J. Biol. Chem.* 265:9583–9586.

Berridge, M. J. 1993. Inositol trisphosphate and calcium signaling. *Nature.* 361:315–324.

Berridge, M. J., and R. F. Irvine. 1989. Inositol phosphates and cell signaling. *Nature.* 341:197–205.

Berstein, G., J. L. Blank, D. Y. Jhon, J. H. Exton, S. G. Rhee, and E. M. Ross. 1992. Phospholipase C-beta 1 is a GTPase-activating protein for Gq/11, its physiologic regulator. *Cell.* 70:411–418.

Bhalla, U. S. 1998. The network within: signaling pathways. *In* The Book of GENESIS: Exploring Realistic Neural Models with the GEneral NEural SImulation System. J.M. Bower and D. Beeman, editors. Springer-Verlag, New York.169–190.

Bhalla, U. S., and R. Iyengar. 1999. Emergent properties of networks of biological signaling pathways. *Science.* 283:381–387.

Bootman, M. D., and M. J. Berridge. 1995. The elemental principles of calcium signaling. *Cell.* 83:675–678.

Chi, H., X. Yang, P. D. Kingsley, R. J. O'Keefe, J. E. Puzas, R. N. Rosier, S. B. Shears, and P. R. Reynolds. 2000. Targeted deletion of Minpp1 provides new insight into the activity of multiple inositol polyphosphate phosphatase in vivo. *Mol. Cell. Biol.* 20:6496–6507.

Communi, D., V. Vanweyenberg, and C. Erneux. 1997. D-Myo-inositol 1,4,5-trisphosphate 3-kinase A is activated by receptor activation through a calcium:calmodulin-dependent protein kinase II phosphorylation mechanism. *EMBO J.* 16:1943–1952.

Cullen, P. J., J. J. Hsuan, O. Truong, A. J. Letcher, T. R. Jackson, A. P. Dawson, and R. F. Irvine. 1995. Identification of a specific $Ins(1,3,4,5)P_4$-binding protein as a member of the GAP1 family. *Nature.* 376:527–530.

Cullen, P. J., R. F. Irvine, and A. P. Dawson. 1990. Synergistic control of Ca^{2+} mobilization in permeabilized mouse L1210 lymphoma cells by inositol 2,4,5-trisphosphate and inositol 1,3,4,5-tetrakisphosphate. *Biochem J.* 271:549–553.

Dolmetsch, R. E., K. Xu, and R. S. Lewis. 1998. Calcium oscillations increase the efficiency and specificity of gene expression. *Nature.* 392: 933–936.

Fukuda, M., and K. Mikoshiba. 1996. Structure-function relationships of the mouse Gap1m: determination of the inositol 1,3,4,5-tetrakisphosphate-binding domain. *J. Biol. Chem.* 271:18838–18842.

Fukuda, M., and K. Mikoshiba. 1997. The function of inositol high polyphosphate binding proteins. *Bioessays.* 19:593–603.

Guse, A. H., E. Greiner, F. Emmrich, and K. Brand. 1993. Mass changes of inositol 1,3,4,5,6-pentakisphosphate and inositol hexakisphosphate during cell cycle progression in rat thymocytes. *J. Biol. Chem.* 268: 7129–7133.

Hansen, C. A., R. A. Johanson, M. T. Williamson, and J. R. Williamson. 1987. Purification and characterization of two types of soluble inositol phosphate 5-phosphomonoesterases from rat brain. *J. Biol. Chem.* 262: 17319–17326.

Harootunian, A. T., J. P. Kao, S. Paranjape, and R. Y. Tsien. 1991. Generation of calcium oscillations in fibroblasts by positive feedback between calcium and IP_3. *Science.* 251:75–78.

Hermosura, M. C., H. Takeuchi, A. Fleig, A. M. Riley, B. V. Potter, M. Hirata, and R. Penner. 2000. $InsP_4$ facilitates store-operated calcium influx by inhibition of $InsP_3$ 5-phosphatase. *Nature.* 408:735–740.

Hirose, K., S. Kadowaki, M. Tanabe, H. Takeshima, and M. Iino. 1999. Spatiotemporal dynamics of inositol 1,4,5-trisphosphate that underlies complex Ca^{2+} mobilization patterns. *Science.* 284:1527–1530.

Ho, M. W., X. Yang, M. A. Carew, T. Zhang, L. Hua, Y. U. Kwon, S. K. Chung, S. Adelt, G. Vogel, A. M. Riley, B. V. Potter, and S. B. Shears. 2002. Regulation of ins(3,4,5,6)p(4) signaling by a reversible kinase/phosphatase. *Curr. Biol.* 12:477–482.

Hoer, A., and E. Oberdisse. 1991. Inositol 1,3,4,5,6-pentakisphosphate and inositol hexakisphosphate are inhibitors of the soluble inositol 1,3,4,5-tetrakisphosphate 3-phosphatase and the inositol 1,4,5-trisphosphate/1,3,4,5-tetrakisphosphate 5-phosphatase from pig brain. *Biochem. J.* 278:219–224.

Hoth, M., and R. Penner. 1992. Depletion of intracellular calcium stores activates calcium current in mast cells. *Nature.* 355:353–356.

Hughes, P. J., and A. H. Drummond. 1987. Formation of inositol phosphate isomers in GH3 pituitary tumor cells stimulated with thyrotropin-releasing hormone. *Biochem. J.* 248:463–470.

Irvine, R. 2001. Inositol phosphates: does IP_4 run a protection racket? *Curr. Biol.* 11:R172–R174.

Irvine, R. F., and M. J. Schell. 2001. Back in the water: the return of the inositol phosphates. *Nat. Rev. Mol. Cell Biol.* 2:327–338.

Jackson, T. R., T. J. Hallam, C. P. Downes, and M. R. Hanley. 1987. Receptor coupled events in bradykinin action: rapid production of inositol phosphates and regulation of cytosolic free Ca^{2+} in a neural cell line. *EMBO J.* 6:49–54.

Jencks, W. P. 1976. Physical and chemical data. *In* Handbook of Biochemistry and Molecular Biology, Vol. I. G.D. Fasman, editor. CRC Press, Boca Raton, FL. 296–304.

Kahlert, S., and G. Reiser. 2000. Requirement of glycolytic and mitochondrial energy supply for loading of Ca(2+) stores and InsP(3)-mediated Ca(2+) signaling in rat hippocampus astrocytes. *J. Neurosci. Res.* 61: 409–420.

Lambert, D. G., and S. R. Nahorski. 1990. Muscarinic-receptor-mediated changes in intracellular Ca^{2+} and inositol 1,4,5-trisphosphate mass in a human neuroblastoma cell line, SH-SY5Y. *Biochem. J.* 265:555–562.

Lechleiter, J., S. Girard, E. Peralta, and D. Clapham. 1991. Spiral calcium wave propagation and annihilation in *Xenopus laevis* oocytes. *Science.* 252:123–126.

Majerus, P. W. 1992. Inositol phosphate biochemistry. *Annu. Rev. Biochem.* 61:225–250.

MacGregor, R. J. 1987. Neural and brain modeling. Academic Press, San Diego, CA.

Meyer, T., and L. Stryer. 1988. Molecular model for receptor-stimulated calcium spiking. *Proc. Natl. Acad. Sci. U. S. A.* 85:5051–5055.

Meyer, T., and L. Stryer. 1991. Calcium spiking. *Annu. Rev. Biophys. Biophys. Chem.* 20:153–174.

Morris, A. P., D. V. Gallacher, R. F. Irvine, and O. H. Petersen. 1987. Synergism of inositol trisphosphate and tetrakisphosphate in activating Ca^{2+}-dependent K^+ channels. *Nature.* 330:653–655.

Nishizuka, Y. 1988. The molecular heterogeneity of protein kinase C and its implications for cellular regulation. *Nature.* 334:661–665.

Nogimori, K., P. J. Hughes, M. C. Glennon, M. E. Hodgson, J. W. Putney, Jr., and S. B. Shears. 1991. Purification of an inositol (1,3,4,5)-tetrakisphosphate 3-phosphatase activity from rat liver and the evaluation of its substrate specificity. *J. Biol. Chem.* 266:16499–16506.

Parker, I., and I. Ivorra. 1991. Inositol tetrakisphosphate liberates stored Ca^{2+} in Xenopus oocytes and facilitates responses to inositol trisphosphate. *J. Physiol.* 433:207–227.

Parker, I., and Y. Yao. 1991. Regenerative release of calcium from functionally discrete subcellular stores by inositol trisphosphate. *Proc. R. Soc. Lond. B Biol. Sci.* 246:269–274.

Pittet, D., W. Schlegel, D. P. Lew, A. Monod, and G. W. Mayr. 1989. Mass changes in inositol tetrakis- and pentakisphosphate isomers induced by chemotactic peptide stimulation in HL-60 cells. *J. Biol. Chem.* 264: 18489–18493.

Rhee, S. G. 2001. Regulation of phosphoinositide-specific phospholipase C. *Annu. Rev. Biochem.* 70:281–312.

Safrany, S. T., and S. B. Shears. 1998. Turnover of bis-diphosphoinositol tetrakisphosphate in a smooth muscle cell line is regulated by beta2-adrenergic receptors through a cAMP-mediated, A-kinase-independent mechanism. *EMBO J.* 17:1710–1716.

Shears, S. B. 1989. Metabolism of the inositol phosphates produced upon receptor activation. *Biochem. J.* 260:313–324.

Shears, S. B. 1998. The versatility of inositol phosphates as cellular signals. *Biochim. Biophys. Acta.* 1436:49–67.

Sim, S. S., J. W. Kim, and S. G. Rhee. 1990. Regulation of D-myo-inositol 1,4,5-trisphosphate 3-kinase by cAMP-dependent protein kinase and protein kinase C. *J. Biol. Chem.* 265:10367–10372.

Sims, C. E., and N. L. Allbritton. 1998. Metabolism of inositol 1,4,5-trisphosphate and inositol 1,3,4,5-tetrakisphosphate by the oocytes of *Xenopus laevis*. *J. Biol. Chem.* 273:4052–4058.

Smith, P. M., A. R. Harmer, A. J. Letcher, and R. F. Irvine. 2000. The effect of inositol 1,3,4,5-tetrakisphosphate on inositol trisphosphate-induced Ca^{2+} mobilization in freshly isolated and cultured mouse lacrimal acinar cells. *Biochem. J.* 347:77–82.

Soriano, S., S. Thomas, S. High, G. Griffiths, C. D'santos, P. Cullen, and G. Banting. 1997. Membrane association, localization and topology of rat inositol 1,4,5-trisphosphate 3-kinase B: implications for membrane traffic and Ca^{2+} homeostasis. *Biochem J.* 324:579–589.

Streb, H., R. F. Irvine, M. J. Berridge, and I. Schulz. 1983. Release of Ca^{2+} from a nonmitochondrial intracellular store in pancreatic acinar cells by inositol-1,4,5-trisphosphate. *Nature.* 306:67–69.

Tang, Y., J. L. Stephenson, and H. G. Othmer. 1996. Simplification and analysis of models of calcium dynamics based on IP_3-sensitive calcium channel kinetics. *Biophys. J.* 70:246–263.

Taylor, C. W., and A. Richardson. 1991. Structure and function of inositol trisphosphate receptors. *Pharmacol. Ther.* 51:97–137.

Tsien, R. W., and R. Y. Tsien. 1990. Calcium channels, stores, and oscillations. *Annu. Rev. Cell. Biol.* 6:715–760.

Vajanaphanich, M., C. Schultz, M. T. Rudolf, M. Wasserman, P. Enyedi, A. Craxton, S. B. Shears, R. Y. Tsien, K. E. Barrett, and A. Traynor-Kaplan. 1994. Long-term uncoupling of chloride secretion from intracellular calcium levels by $Ins(3,4,5,6)P_4$. *Nature.* 371:711–714.

Vallejo, M., T. Jackson, S. Lightman, and M. R. Hanley. 1987. Occurrence and extracellular actions of inositol pentakis- and hexakisphosphate in mammalian brain. *Nature.* 330:656–658.

Voglmaier, S. M., M. E. Bembenek, A. I. Kaplin, G. Dorman, J. D. Olszewski, G. D. Prestwich, and S. H. Snyder. 1996. Purified inositol hexakisphosphate kinase is an ATP synthase: diphosphoinositol pentakisphosphate as a high-energy phosphate donor. *Proc. Natl. Acad. Sci. U.S.A.* 93:4305–4310.

Wakui, M., B. V. Potter, and O. H. Petersen. 1989. Pulsatile intracellular calcium release does not depend on fluctuations in inositol trisphosphate concentration. *Nature.* 339:317–320.

Wang, S. S., A. A. Alousi, and S. H. Thompson. 1995. The lifetime of inositol 1,4,5-trisphosphate in single cells. *J. Gen. Physiol.* 105: 149–171.

Yang, X., M. Rudolf, M. A. Carew, M. Yoshida, V. Nerreter, A. M. Riley, S. K. Chung, K. S. Bruzik, B. V. Potter, C. Schultz, and S. B. Shears. 1999. Inositol 1,3,4-trisphosphate acts in vivo as a specific regulator of cellular signaling by inositol 3,4,5,6-tetrakisphosphate. *J. Biol. Chem.* 274:18973–18980.

Yang, X., and S. B. Shears. 2000. Multitasking in signal transduction by a promiscuous human Ins(3,4,5,6)P(4) 1-kinase/Ins(1,3,4)P(3) 5/6-kinase. *Biochem J.* 351:551–555.

Ye, W., N. Ali, M. E. Bembenek, S. B. Shears, and E. M. Lafer. 1995. Inhibition of clathrin assembly by high affinity binding of specific inositol polyphosphates to the synapse-specific clathrin assembly protein AP-3. *J. Biol. Chem.* 270:1564–1568.

Zhu, D. M., E. Tekle, C. Y. Huang, and P. B. Chock. 2000. Inositol tetrakisphosphate as a frequency regulator in calcium oscillations in HeLa cells. *J. Biol. Chem.* 275:6063–6066.